Computer-Aided Design 189 (2025) 103937

Contents lists available at ScienceDirect

Computer-Aided Design

journal homepage: www.elsevier.com/locate/cad

Discrete isogonal nets with similar parallelograms

Hui Wang [a,*], Xinye Li [b], Zhi Li [c], Cheng Wang [d]

[a] School of Mathematics and Statistics, Xi'an Jiaotong University, China
[b] College of Civil Engineering, Tongji University, China
[c] School of Engineering, RMIT University, Australia
[d] School of Computing Sciences, University of East Anglia, UK

ARTICLE INFO

Keywords:
Isogonal nets
Isogonal webs
Checkerboard pattern
Discrete differential geometry
Conformal parametrization
Mesh optimization
Computational design
High-quality quad mesh

ABSTRACT

High-quality surface designs are increasingly significant in industrial applications, such as architecture and product design, yet they pose challenges in balancing visual appeal and functional requirements. Isogonal nets (I-nets) stand out for their aesthetically pleasing patterns and engineering practicality. However, constructing such nets remains difficult due to their dependence on complex angle constraints or a narrow focus on orthogonal scenarios. We propose a novel representation and construction method for I-nets characterized by similar mid-edge subdivided parallelograms in the quad faces. This approach achieves a simple yet versatile representation that generalizes orthogonal nets and extends to the construction of isogonal 4-webs (I-webs). By focusing on constraining edge ratios, our method enables efficient integration into mesh optimization algorithms. We demonstrate the effectiveness of I-nets and I-webs in freeform shapes through conformal mapping and numerical optimization. Experiments on various surfaces validate our method, showcasing its potential for both theoretical advancements and practical applications.

1. Introduction

High-quality surfaces are typically designed not only to satisfy functional requirements but also to possess unique visual effects. The design of such surfaces relies on *curve nets* that form nearly uniform angles between the curves [1]. In recent years, surfaces generated by these nets have been widely used in architectural facades [2] and shell structures [3], where the design of discrete panels in the structures follows the curve nets to achieve aesthetically pleasing and functional designs.

Among all curved nets, *orthogonal nets* are the key special case where two families of curves intersect at right angles. These nets have attracted extensive attention from researchers and designers, as they can serve as foundational structures for the construction of other specialized quad nets [4]. For instance, they align with principal directions [5], which enables the construction of principal curvature nets and simplifies curvature analysis. Additionally, due to their right angle constraints, orthogonal nets streamline panel layouts for architectural envelopes, thereby reducing manufacturing complexity and assembly costs [6].

However, many practical design scenarios require greater geometric flexibility. For instance, freeform architectures often feature sweeping curves and intricate transitions that cannot be captured by strictly perpendicular curve families. In these contexts, *isogonal nets* present a compelling alternative. By allowing a constant intersection angle that does not have to be 90 degrees, I-nets give designers and engineers more flexibility in shaping their creations. This flexibility is particularly valuable for architectural facades, shell structures, and product design, where unique visual effects and adaptable structural layouts are crucial.

Recently, I-nets have started to gain increasing attention in both research and industry for advanced surface design, serving as fundamental structures for other specialized nets. For instance, isogonal asymptotic nets characterize surfaces with negative constant ratios of principal curvatures (CRPC-nets) and are instrumental in designing gridshell structures composed of straight and developable lamellas [7–9]. Isogonal conjugate principal symmetric nets (S-nets) characterize positive CRPC-nets [9]. Moreover, isogonal S-nets with constant normal curvatures represent affine linear Weingarten surfaces, enabling cost-effective paneling of freeform surfaces using curvature-equivalent panels [10,11]. Additionally, combining I-nets with another family of curves can form triangular or hexagonal patterns. For example, integrating geodesic curves with negative CRPC-nets has been shown to be effective in constructing large-scale gridshells. This approach ensures congruent elementary nodes and lamellas while assuring structural stability, which are essential for structural integrity and aesthetic consistency [12,13].

* Corresponding author.
E-mail address: huiwang@xjtu.edu.cn (H. Wang).

https://doi.org/10.1016/j.cad.2025.103937
Received 7 June 2025; Received in revised form 10 July 2025; Accepted 22 July 2025
Available online 11 August 2025
0010-4485/© 2025 Elsevier Ltd. All rights are reserved, including those for text and data mining, AI training, and similar technologies.

Despite the tremendous potential of I-nets, their construction methods still face significant limitations in optimization complexity and mesh analysis. Existing approaches can be generally categorized into two categories: *constraining angle between net diagonals* or *constraining angle net medial lines*. The former focuses on maintaining a constant angle between diagonals, thereby emphasizing the diagonal meshes over the original control mesh [8,9,14,15], which makes the direct analysis less intuitive and less practical for real-world applications. The latter enforces constant angles between curve tangents, which requires representing two unit tangent vectors and introducing auxiliary variables for their norms and unit vectors [9–11,16,17]. This not only increases the complexity of mesh optimization problems and hinders efficient implementation but also complicates the analysis of geometric invariance properties.

To address these challenges, we propose a novel definition and construction of I-nets based on the *Checkerboard Pattern* method [18]. Our approach focuses on developing I-nets with a simple representation and efficient implementation, prioritizing visual regularity and practical usability. We summarize our contributions as follows:

- We propose a simple representation approach for I-nets, fully compatible with existing orthogonal and isogonal net definitions, characterized by similar mid-edge subdivided parallelograms.
- I-nets are defined by two constant edge ratios, which can be easily integrated into mesh optimization algorithms.
- We introduce the concept of isogonal 4-webs (*I-webs*), a novel framework that has not been previously explored.
- We demonstrate the versatility of I-nets and I-webs in high-quality surface design through conformal mapping and numerical optimization.

The structure of this paper is organized as follows. Section 2 reviews related work on I-nets. Section 3 examines the relationship between the angles and edge ratios of a parallelogram and explores 2D conformal mapping. Section 4 introduces the proposed I-nets in both smooth and discrete theories, including special cases compatible with orthogonal nets. The theory for representing I-webs is also developed. Section 5 details the construction of I-nets on Kinematic surfaces. Section 6 presents the optimization methods of I-nets. Finally, conclusions and future research directions are discussed in Section 7.

2. Related work

I-nets represent a generalization of orthogonal nets, where the constant angle is not restricted to 90 degrees. In the construction of isogonal quad meshes, two primary methods exist for defining a constant angle locally on each quad face by considering the subdivided parallelograms. These methods can generally be divided into two categories: constraining the angle between quad mesh diagonals, and constraining the angle between quad mesh medial lines on each quad face of the mesh.

Before discussing the differences between these existing methods and our proposed approach, we first introduce the checkerboard pattern method, which serves as the foundation for our work.

Checkerboard Pattern A quad mesh, where every second face is a parallelogram (referred to as the black quad) and the alternate face is a general quad (referred to as the white quad), is known as a *Checkerboard Pattern (CBP)*, first introduced in [18]. Any general quad mesh can be converted into a CBP through mid-edge subdivision of each quad face, resulting in inscribed planar quads that are *parallelograms*. The CBP is also seen as a quad mesh refinement in the diagonal direction [19]. Its curvature theory can be discussed based on the definitions of shape operators provided in [20]. The exploration of CBPs in general quad meshes has revealed significant benefits across various fields, including geometry processing and architectural structures. Applications include isometric shape deformations [15], mesh parametrizations [14], transformable design [18] and mechanisms [21], as well as architectural skins [11] and support structures of gridshells [8].

Constant angle between mesh diagonals. The mid-edge subdivided parallelograms of the mesh quads are treated as first-order faces of the control quad mesh, with their edges representing discrete first-order derivatives [20]. These parallelogram edges are parallel to the diagonals of the original control mesh, which also form the edges of two diagonal meshes. As a result, the edges of the diagonal mesh are uniquely determined by the CBP. The two diagonal meshes create a mesh pairing in the diagonal direction of the control mesh. A mesh is orthogonal if this pairing is rhombic [4], while an isogonal mesh is defined by a constant angle between the mesh pairing [8,9,14,15]. This approach prioritizes the diagonal mesh over the original control mesh, making it less convenient for directly analyzing a given mesh.

Constant angle between mesh medial lines. The two diagonals of each inscribed parallelogram serve as medial lines of the control quad and are interpreted as discrete second-order derivatives at the quad face barycenter. Constraining the angle between these medial lines to be constant enforces an isogonal structure on the quad mesh, as shown in [9]. However, this approach requires representing two unit tangent vectors, which complicates the standard optimization problem by introducing auxiliary variables for norms and unit vectors [22].

Specifically, discrete orthogonality can be simply represented by equal diagonal lengths within each quad, where the ratios between diagonal lengths are 1. This is a consequence of the properties of mid-edge subdivided rhombuses, where the inscribed parallelograms transform into rhombuses [4]. This approach demonstrates advantages in the handling the boundary alignment, implementation of simple quadratic equations and compatible constructions of various classical nets [4], which are commonly discussed in the context of Discrete Differential Geometry [23].

However, directly generalizing the constraint that the ratio of the two diagonal lengths should be constant but not equal to 1 does not ensure a constant angle between the medial lines, as there remains one degree of freedom, specifically an interior angle of the parallelogram. Consequently, we introduce an additional constraint: a constant ratio between the medial lines.

The combination of a constant ratio between the diagonals of the quad mesh and a constant ratio between the medial lines effectively determines the shape of the inscribed parallelograms. This ensures that both the interior angles and the diagonal angles of all parallelograms are constant—and specifically, equal. Thus, we construct an I-net characterized by a constant angle between the diagonals and another constant angle between the medial lines. This implies the presence of similar inscribed parallelograms within the mesh, thereby forming an isogonal 4-web.

Similar parallelograms. We define the I-net by quad meshes with similar parallelograms in the CBP. We seek to describe similar parallelograms by constraining the ratios of their edges, rather than representing angles. This geometric constraint, which focuses on the edges rather than the angles, can be readily integrated into numerical optimization procedures. A simple example of such an I-net is a planar sheared regular grid, although our focus is on general spatial nets.

Special cases occur when the parallelograms take specific shapes, such as rhombuses, rectangles, or squares. These shapes define discrete orthogonal nets compatible with previous work [4,8,18].

A notable special case arises when the interior angle of a parallelogram equals its diagonal angle. This implies that the constant angle between the quad diagonals is equal to the constant angle between the medial lines. We demonstrate that this angle condition can be prescribed by a single constant edge ratio, simplifying both the isogonal representation and the optimization process.

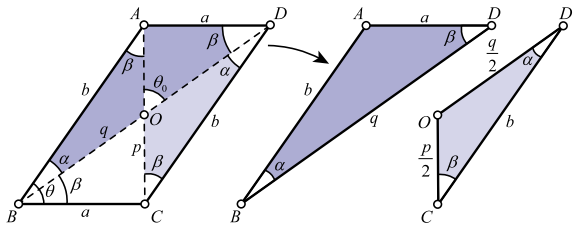

Fig. 1. A (θ,θ_0)−parallelogram with an interior angle θ and an diagonal angle θ_0. If $\theta=\theta_0$, it is a θ−parallelogram, which possesses two similar triangles $\triangle\, ABD \simeq \triangle\, ODC$ with equal edge ratios $a:b:q=\frac{p}{2}:\frac{q}{2}:b$.

3. Parallelogram determined by two edge ratios

In this section, we examine the relationship between the angles and edge ratios of a parallelogram, including the special case where the interior angle equals the diagonal angle. Conformal mapping results in 2D are explored for a planar sheared grid with congruent parallelograms, demonstrating the geometry-invariant property under conformal maps.

3.1. Parallelogram prescribed by an interior angle and a diagonal angle

A parallelogram is a special type of planar quad with equal and parallel opposite sides. It exhibits several distinct properties: equal opposite angles, supplementary adjacent angles, and diagonals that bisect each other.

Special cases arise when additional constraints are applied: If the lengths of two adjacent sides are equal, the parallelogram becomes a rhombus, where the diagonals are perpendicular to each other. If the lengths of two diagonals are equal, the parallelogram is a rectangle. If both conditions are met (equal adjacent sides and equal diagonals), it transforms into a square, where all interior angles are $\frac{\pi}{2}$ and the diagonals are of equal length.

Interior angle θ. Given a parallelogram $ABCD$ with neighboring edge lengths $BC=a$ and $AB=b$ and their interior angle $\angle B=\theta$, the lengths of the two diagonal $AC=p$ and $BD=q$ can be expressed using the Law of Cosine in trigonometry as follows (Fig. 1):

$$p^2=a^2+b^2-2ab\cos\theta, q^2=a^2+b^2+2ab\cos\theta, \tag{1}$$

which brings to

$$p^2+q^2=2(a^2+b^2). \tag{2}$$

Diagonal angle θ_0. Suppose an angle between the two diagonals of a parallelogram ABCD is $\angle AOD=\theta_0$, where O is the intersection of two diagonals. The diagonal angle θ_0 is generally not equal to the interior angle θ. For instance, in a rhombus, $\theta_0=\frac{\pi}{2}$, but only when the rhombus becomes a square does $\theta=\frac{\pi}{2}$.

(θ,θ_0)−parallelogram. A parallelogram is referred to as an *(θ,θ_0)−parallelogram* when its interior angle is denoted by θ and its diagonal angle by θ_0.

Neighboring edge ratio λ and diagonal edge ratio μ. To simplify the task of analyzing the shape of a parallelogram, we assign the lengths of the neighboring edges as $a=1$ and $b=\lambda$ and the lengths of the diagonal edge as p and $q=\mu p$. This results in the expression for p as $p=\sqrt{\frac{2(1+\lambda^2)}{1+\mu^2}}$, derived from Eq. (2). The ratios $a:b:p:q=1:\lambda:\sqrt{\frac{2(1+\lambda^2)}{1+\mu^2}}:\mu\sqrt{\frac{2(1+\lambda^2)}{1+\mu^2}}$ are unique, indicating that the shape of the parallelogram is uniquely determined by the ratios λ and μ. Given λ and μ, the parallelogram's shape will fixed, with only its scalar varying.

Lemma 1. *For a (θ,θ_0)−parallelogram with two edge lengths $a=1$ and $b=\lambda$ and two diagonal lengths p and q, the interior angles θ and the diagonal angle θ_0 can be expressed in terms of λ and μ as follows:*

$$\cos\theta=\frac{(1+\lambda^2)(\mu^2-1)}{2\lambda(1+\mu^2)}, \cos\theta_0=\frac{(1+\mu^2)(\lambda^2-1)}{2\mu(1+\lambda^2)}, \tag{3}$$

where λ and μ satisfy the conditions:

$$\frac{|\mu-1|}{\mu+1}<\lambda<\frac{\mu+1}{|\mu-1|}, \frac{|\lambda-1|}{\lambda+1}<\mu<\frac{\lambda+1}{|\lambda-1|}. \tag{4}$$

Additionally, the angles α and β of the triangle forming half of the parallelogram can be computed by λ and μ as follows:

$$\cos\alpha=\frac{3\lambda^2\mu^2+\lambda^2+\mu^2-1}{2\lambda\mu\sqrt{2(1+\lambda^2)(1+\mu^2)}}, \cos\beta=\frac{\lambda^2\mu^2-\lambda^2+3\mu^2+1}{2\mu\sqrt{2(1+\lambda^2)(1+\mu^2)}}. \tag{5}$$

Proof. From Eq. (1), where $p=\sqrt{\frac{2(1+\lambda^2)}{1+\mu^2}}$ and $q=\mu p$, the cosines of the angles θ and θ_0 are derived and presented in Eq. (3). The ratios λ and μ must satisfy the conditions specified in Eq. (4) within $\triangle\, ABC$, where the edge length are $1,\lambda$ and $\sqrt{\frac{2(1+\lambda^2)}{1+\mu^2}}$. These conditions are consistent with the constraints imposed by the cosine rule, ensuring that $\cos\theta$ and $\cos\theta_0$ fall within the interval $(-1,1)$. The angles α and β can be computed from half of a parallelogram as a triangle with edge lengths $1,\lambda$, and $q=\mu\sqrt{\frac{2(1+\lambda^2)}{1+\mu^2}}$.

The ratios λ and μ serve analogous functions in determining the shape of the parallelogram, and exhibit a mirrored similarity with respect to their reciprocals.

If μ is held constant while the ratio of neighboring edges is inverted such that $a=1$ and $b=\frac{1}{\lambda}$, the interior angle θ remains unchanged, whereas the diagonal angle θ_0 transforms into $\pi-\theta_0$. Fig. 2-(B) shows a parallelogram with edge ratios $(b:a,q:p)=(\frac{1}{\lambda},\mu)$.

Conversely, if the ratio of the diagonal lengths is inverted such that $p=\mu q$, then θ transforms into $\pi-\theta$, while θ_0 remains unchanged. The resulting parallelogram in Fig. 2-(C), with edge ratios $(b:a,q:p)=(\lambda,\frac{1}{\mu})$, is a mirror image of the original in Fig. 2-(A) and is similar to the scaled version in Fig. 2-(B) with a scaling factor of $\frac{1}{\lambda}$.

In particular, when $(b:a,q:p)=(\frac{1}{\lambda},\frac{1}{\mu})$, both θ and θ_0 transition to their respective supplementary angles. This transformed parallelogram in Fig. 2-(D) is similar to the original in Fig. 2-(A), scaled down by a factor of $\frac{1}{\lambda}$ and mirrored to the one in Fig. 2-(B). This illustrates the symmetrical influence of λ and μ on the geometry of the parallelogram.

Additionally, if $\lambda>1$ or $\mu>1$, the angles θ_0 or θ are acute, respectively. Specially, if $\lambda=1$ or $\mu=1$, then $\theta_0=\frac{\pi}{2}$ or $\theta=\frac{\pi}{2}$, respectively. For $\mu>1$, this implies that angle θ is acute and diagonal BD is longer than AC, the range for λ is then given by:

$$\frac{\mu-1}{\mu+1}<\lambda<\frac{\mu+1}{\mu-1}, (\mu>1). \tag{6}$$

This condition facilitates the simplification of our discussion regarding the shapes of parallelograms, focusing solely on the configurations depicted in Fig. 2-(A,B), where θ is acute.

3.2. Parallelogram with an interior angle equal to a diagonal angle

When the interior angle θ remains constant, the diagonal angle θ_0 decreases as λ increases. There must be a point at which $\theta=\theta_0$, which makes $\lambda=\mu$. At this point, the shape of the parallelogram is solely determined by λ.

Definition 2. A parallelogram is called a *θ−parallelogram* if the interior angle θ is equal to the angle between the two diagonals.

For a θ−parallelogram with two edge lengths $a=1$ and $b=\lambda$ and two diagonal lengths p and q, the following properties are exhibited:

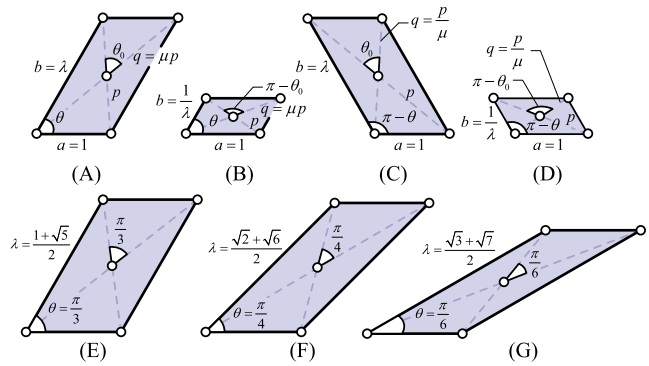

Fig. 2. (A–D) (θ, θ_0)−parallelograms with different edge ratios $(b : a, q : p)$: (A) (λ, μ), (B) $(\frac{1}{\lambda}, \mu)$, (C) $(\lambda, \frac{1}{\mu})$, (D) $(\frac{1}{\lambda}, \frac{1}{\mu})$. (E–G) θ−parallelograms with $\theta = \frac{\pi}{3}, \frac{\pi}{4}$, and $\frac{\pi}{6}$, respectively.

$$p = \sqrt{2}, q = \sqrt{2}\lambda, \tag{7}$$

$$\cos\theta = \frac{1}{2}(\lambda - \frac{1}{\lambda}), \tag{8}$$

$$\sqrt{2} - 1 < \lambda < \sqrt{2} + 1, \tag{9}$$

$$\cos\alpha = \frac{\sqrt{2}(3\lambda^2 - 1)}{4\lambda^2}, \cos\beta = \frac{\sqrt{2}(1 + \lambda^2)}{4\lambda}. \tag{10}$$

The proof of Eqs. (7)–(10) is provided in Appendix A.1.

When $\lambda = 1$, angle $\theta = \frac{\pi}{2}$ indicating the parallelogram is a square. This represents a special case of discrete orthogonality as discussed in [18]. When $\lambda = \frac{1}{a}$, the angle $\theta = \arccos(\frac{1}{2}(\frac{1}{a} - a)) = \pi - \arccos(\frac{1}{2}(a - \frac{1}{a}))$, which implies that the interior angles of two θ−parallelograms, whose side length ratios are reciprocals of each other, are supplementary. This corresponds to the case $(b : a, q : p) = (\frac{1}{\lambda}, \frac{1}{\mu})$ in Fig. 2-(D). For instance, the angle $\theta = \arccos\frac{3}{4}$ and $\theta = \pi - \arccos\frac{3}{4}$ correspond to $\lambda = 2$ and $\lambda = \frac{1}{2}$, respectively.

Given θ, the ratio λ can be calculated directly from Eq. (8) as $\lambda = \cos\theta + \sqrt{1 + \cos^2\theta}$. For example, the ratios λ are $\frac{1+\sqrt{5}}{2}$, $\frac{\sqrt{2}+\sqrt{6}}{2}$, and $\frac{\sqrt{3}+\sqrt{7}}{2}$ for $\theta = \frac{\pi}{3}, \frac{\pi}{4}$, and $\frac{\pi}{6}$, respectively, as seen in Fig. 2.

3.3. Planar sheared grid and its conformal mappings

A planar rectangular grid M can be mapped into a sheared grid M_0 with a specified angle θ_0 through a shear transformation ω, which is a kind of affine mapping. When considering the grids within the complex plane $\mathbb{C}$, the shear transformation ω can be represented as

$$\omega : z = x + iy \mapsto z_\omega = u(x, y) + iv(x, y),$$

where i is the imaginary unit with $i^2 = -1$ and

$$[u, v] = [x, y]\begin{bmatrix} 1 & 0 \\ \cot\theta_0 & 1 \end{bmatrix} = [x + y\cot\theta_0, y].$$

This transformation shears the grid in the horizontal direction, mapping all rectangles to regular parallelograms with an interior angle θ_0 and a diagonal angle supposed θ. There exist multiple parallelograms that can be combined in any manner to form bigger parallelograms, which are similar to each other. These parallelograms are referred to as (θ_0, θ)−parallelograms, and their shape is flexible, depending on the chosen values of θ_0 and θ. Their mid-edge subdivision forms congruent (θ, θ_0)−parallelograms.

The sheared grid M_0 exhibit isogonal properties, characterized by a constant angle θ_0 between their isolines and a constant angle θ between the diagonal lines. For simplicity, we consider the conformal mappings of M_0 with the special case that $\theta_0 = \theta$.

Conformal mappings. A smooth complex mapping $\omega : D \subset \mathbb{C} \mapsto \mathbb{C}; (x, y) \mapsto u(x, y) + iv(x, y)$ is *conformal* if ω is an immersion and angle-preserving. Analytically, conformal mapping ω satisfies the *Cauchy-Riemann equations* that is $u_x = v_y, u_y = -v_x$, which says ω is *holomorphic*. Conformal mappings have variety of applications [24] in cartography, parametrization, texture mapping, remeshing, surface deformation, simulations, and auxetic metamaterials.

If a conformal mapping ω is applied to the grid M_0, two families of straight lines can be transformed into two new families of curves (or lines) that intersect at an angle θ characterized by the tangents between the two families of curves, as seen in Fig. 3. The resulting curvilinear quads will not be congruent but will exhibit similarity. This similarity is not immediately obvious due to their curved boundaries. However, it can be characterized by the mid-edge subdivided parallelograms of the original straight quads, formed by connecting vertices with straight edges. On an infinitesimal scale, these straight quads, shown in Fig. 3-(A'–C') and indicated by gray dashed lines, resemble curvilinear quads, which are depicted by black curves. Their mid-edge subdivided parallelograms are also θ−parallelogram, as ω preserves angles.

Two different conformal mappings $\omega = \frac{1}{z}$ and $\omega' = z^2$ are provided as examples in Fig. 3. The function $\omega = \frac{1}{z}$ is analytic in the complex plane except at $z = 0$, while $\omega' = z^2$ is analytic everywhere in the complex plane. The pre-images (A, B, C) are in the upper half-plane and are mapped into curved grids (A', B', C'), respectively. As shown in Fig. 3-$(C_1 - C_3)$, a sheared grid under different conformal mappings transforms into curved grids with varying shapes, yet the parallelograms within these grids remain similar. For further details on the representation of the sheared grid and their conformal mappings, refer to Appendix A.2.

Remark. The examples above describe two elementary conformal mappings in two-dimensional space. These mappings can be extended to complex mappings by combining various algebraic representations. This approach can also be applied to three-dimensional space. The existence of conformal mappings between surfaces depends on their topology, specifically, there is always a conformal mapping between surfaces that possess disk topology or sphere topology [25]. According to Liouville's theorem [26], the conformal mappings in dimensions 3 and higher are *Möbius transformations* [27].

4. I-net characterized by similar parallelograms in the CBP

We aim to represent and construct I-nets based on a quad mesh characterized by similar parallelograms in the CBP. We start by analyzing a spatial quad defined by its mid-edge subdivided parallelogram. We then examine the conditions for forming an I-net by considering a smooth parametrization $\mathbf{X}(u, v)$ and its diagonal parametrization $\mathbf{Y}(u, v)$, which have constant norm ratios of their tangents. On an infinitesimal scale, $\frac{1}{2}\mathbf{Y}(u, v)$ acts as a CBP of $\mathbf{X}(u, v)$, featuring similar mid-edge subdivided parallelograms. This process results in both $\mathbf{X}(u, v)$ and $\mathbf{Y}(u, v)$ being isogonal, naturally extending to the formation of an I-web—a network of four families of curves that intersect at constant angles. Finally, we explore the discretized counterparts of these theories, ensuring that the discrete representations maintain the key features of both I-nets and I-webs.

4.1. Mid-edge subdivided parallelogram

In a general spatial quad, as shown in Fig. 4, we can consider two types of edge angles. One is the angle θ between the diagonal vectors $\mathbf{d}_1$ and $\mathbf{d}_2$ of the quad. Another is the angle θ_0 between the medial-line vectors $\mathbf{m}_{13}$ and $\mathbf{m}_{24}$ of the quad. By sequentially connecting the midpoints of the quad edges in a counterclockwise direction, we construct a subdivided parallelogram nested within the quad, as it features two pairs of opposite edges that are equal in length and parallel to $\mathbf{d}_1$ and $\mathbf{d}_2$, respectively. The parallelogram is sometimes called *Varignon*

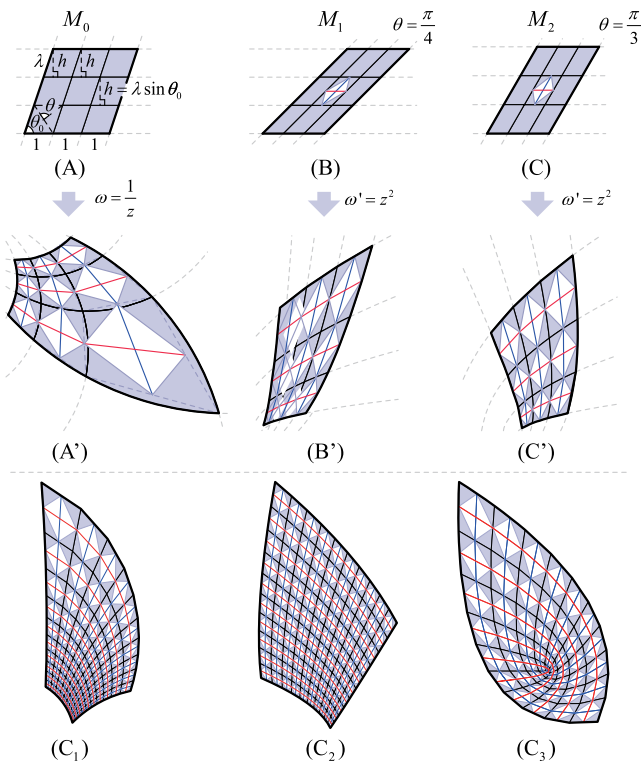

Fig. 3. (A–C) Regular sheared grids M_0, M_1 and M_2 with congruent parallelograms in the upper half-plane mapped from rectangular grids. (B) Sheared grid M_1 with $\theta_0 = \theta = \frac{\pi}{4}$. (C) Sheared grid M_2 with $\theta_0 = \theta = \frac{\pi}{3}$. Conformal mappings of these grids: (A') The mapping $\omega = \frac{1}{z}$ transforms the straight lines of M_0 into circular arcs. (B'–C') The mapping $\omega' = z^2$ transforms M_1 and M_2 into curvilinear grids of parabolas. A ten by ten sheared grid with $\theta_0 = \theta = \frac{\pi}{3}$ is mapped to: (C_1) under $\omega = \frac{1}{z}$, (C_2) and (C_3) under $\omega' = z^2$, forming CBPs with similar $\frac{\pi}{3}$−parallelograms. The difference between (C_2) and (C_3) is that the origin lies within the pre-image of the sheared grid for (C_3).

parallelogram from *Varignon's theorem* [18,28]. Consequently, the angle θ is equivalent to an interior angle of the parallelogram, while the angle θ_0 is the angle between the two diagonals of this parallelogram.

The parallelogram is a (θ, θ_0)−parallelogram with an interior angle θ and a diagonal angle θ_0. Let λ be the ratio of the diagonal lengths, such that $\|\mathbf{d}_2\|/\|\mathbf{d}_1\| = \lambda$, and μ be the ratio of the lengths of the medial lines, that is $\|\mathbf{m}_{13}\|/\|\mathbf{m}_{24}\| = \mu$. The shape of the parallelogram is determined by the angles θ and θ_0, which are the functions of λ and μ as derived from Eq. (3).

Definition 3. A quad is called a $(\theta(\lambda,\mu), \theta_0(\lambda,\mu))$*−quad*, short as (θ, θ_0)*−quad*, if its mid-edge subdivided parallelogram is a (θ, θ_0)−parallelogram.

Proposition 4. *For a (θ, θ_0)−quad with two diagonal vectors $\mathbf{d}_1$ and $\mathbf{d}_2$ and two medial-line vectors $\mathbf{m}_{13}$ and $\mathbf{m}_{24}$, let λ and μ be the ratios of the quad's two diagonal lengths and two medial lines, respectively, given by*

$$\frac{\|\mathbf{d}_2\|}{\|\mathbf{d}_1\|} = \lambda, \tag{11}$$

$$\frac{\|\mathbf{m}_{13}\|}{\|\mathbf{m}_{24}\|} = \mu, \tag{12}$$

the values of λ and μ satisfy Eq. (6).

When $\theta = \theta_0$, it indicates that the angle between the quad's diagonals is equal to the angle between its medial lines. Furthermore, the parallelogram is a θ−parallelogram with θ satisfying Eq. (8). This indicates that the shape of the inscribed parallelogram is solely determined by the ratio of two diagonal lengths.

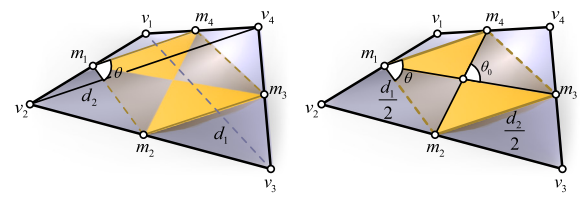

Fig. 4. Mid-edge subdivided parallelogram within a general spacial (θ, θ_0)−quad. The interior angle θ and the diagonal angle θ_0 of the parallelogram are functions of the ratio λ of the diagonal lengths and the ratio μ of the medial-line lengths of the quad. The quad is referred to as a θ−quad, if the parallelogram is a θ−parallelogram, where the angles $\theta = \theta_0$.

Definition 5. A quad is called a $\theta(\lambda)$*−quad*, short as θ*−quad*, if its mid-edge subdivision is a θ−parallelogram, where λ is the ratio of the quad's two diagonal lengths.

A θ−quad exhibits simplified relations between the two diagonal vectors as discussed in the following proposition.

Proposition 6. *Consider a spatial quad with two diagonal vectors $\mathbf{d}_1$ and $\mathbf{d}_2$, where the angle between $\mathbf{d}_1$ and $\mathbf{d}_2$ is θ and the ratio of their lengths is λ as defined by Eq. (11). The quad is a θ−quad if and only if the diagonals satisfy*

$$\mathbf{d}_2^2 - \mathbf{d}_1^2 = 2\mathbf{d}_1 \cdot \mathbf{d}_2. \tag{13}$$

Proof. $\Rightarrow$ The dot product $\mathbf{d}_1 \cdot \mathbf{d}_2$ is equal to $\|\mathbf{d}_1\|\|\mathbf{d}_2\|\cos\theta = \|\mathbf{d}_1\|^2\lambda\cos\theta$. Since θ is a function of λ, substituting $\cos\theta$ from Eq. (8) yields $\mathbf{d}_1 \cdot \mathbf{d}_2 = \frac{\mathbf{d}_2^2 - \mathbf{d}_1^2}{2}$, which is Eq. (13).

$\Leftarrow$ The area of a parallelogram A can be expressed as $A = \|\mathbf{d}_1 \times \mathbf{d}_2\| = \|\mathbf{d}_1\|\|\mathbf{d}_2\|\sin\theta$. Alternatively, from the diagonal point of view, the area can also be calculated as $A = \frac{1}{2}\|(\mathbf{d}_1 + \mathbf{d}_2) \times (\mathbf{d}_2 - \mathbf{d}_1)\| = \frac{1}{2}\|\mathbf{d}_1 + \mathbf{d}_2\|\|\mathbf{d}_2 - \mathbf{d}_1\|\sin\theta_0$, where θ_0 is the angle between the medial lines of the quad. From the equality of these expressions, we derive $\frac{\|\mathbf{d}_1+\mathbf{d}_2\|\|\mathbf{d}_2-\mathbf{d}_1\|}{2\|\mathbf{d}_1\|\|\mathbf{d}_2\|} = \frac{\sin\theta}{\sin\theta_0}$. Eq. (13) can be formulated as $\|\mathbf{d}_1+\mathbf{d}_2\|\|\mathbf{d}_2-\mathbf{d}_1\|\cos\theta_0 = 2\|\mathbf{d}_1\|\|\mathbf{d}_2\|\cos\theta$, which leads to $\frac{\|\mathbf{d}_1+\mathbf{d}_2\|\|\mathbf{d}_2-\mathbf{d}_1\|}{2\|\mathbf{d}_1\|\|\mathbf{d}_2\|} = \frac{\cos\theta}{\cos\theta_0}$. Consequently, we have $\frac{\sin\theta}{\sin\theta_0} = \frac{\cos\theta}{\cos\theta_0}$, which is equivalent to $\sin(\theta - \theta_0) = 0$. Thus $\theta = \theta_0$ with the reasonable range of $\theta, \theta_0 \in (0, \pi)$. This indicates that Eq. (13) ensures the interior angle θ is equal to the angle θ_0 between the diagonals in a parallelogram.

4.2. Isogonal net and web

Before constructing the discrete isogonal net with (θ, θ_0)− quads, we discuss the corresponding smooth theory, which shows close relationship involving isogonal web involving four families of curves.

Given a smooth parametrization $\mathbf{X} : (u, v) \subset \mathbb{R}^2 \mapsto \mathbf{X}(u, v) \subset \mathbb{R}^3$, the condition for the parameter lines to form equal angles is that the angle between the partial derivatives $\mathbf{X}_u$ and $\mathbf{X}_v$ is constant. There exists a diagonal parametrization $\mathbf{Y}(u, v)$ defined by $\mathbf{Y}(u, v) = \mathbf{X}(u - v, u + v)$, where the partial derivatives $\mathbf{Y}_u = \mathbf{X}_u - \mathbf{X}_v$ and $\mathbf{Y}_v = \mathbf{X}_u + \mathbf{X}_v$. The two parameterizations $\mathbf{X}(u, v)$ and $\mathbf{Y}(u, v)$ form a web of four families of curves (4-web), that are combinatorially equivalent to the families $u = const.$, $v = const.$, $u + v = const.$ and $u - v = const.$ of straight lines in the uv plane, as seen in Fig. 5.

On an infinitesimal scale, the two parameter lines of $\mathbf{Y}(u, v)$ lead to mid-edge subdivided parallelograms with edge vectors $\frac{\mathbf{Y}_u}{2}$ and $\frac{\mathbf{Y}_v}{2}$, and diagonal vectors $\mathbf{X}_u$ and $\mathbf{X}_v$. The isogonal net and web of the surface can be analyzed using these parallelograms, leading to the following lemma.

Theorem 7. *A smooth parametrization $\mathbf{X} : (u, v) \subset \mathbb{R}^2 \mapsto \mathbf{X}(u, v) \subset \mathbb{R}^3$ is isogonal (I-net) if the ratios $\frac{\|\mathbf{X}_u\|}{\|\mathbf{X}_v\|}$ and $\frac{\|\mathbf{Y}_v\|}{\|\mathbf{Y}_u\|}$ are constant, where $\mathbf{Y}(u, v) = \mathbf{X}(u-v, u+v)$ is the diagonal parametrization of $\mathbf{X}(u, v)$. Furthermore, $\mathbf{Y}(u, v)$ is isogonal with respect to $\mathbf{X}(u, v)$.*

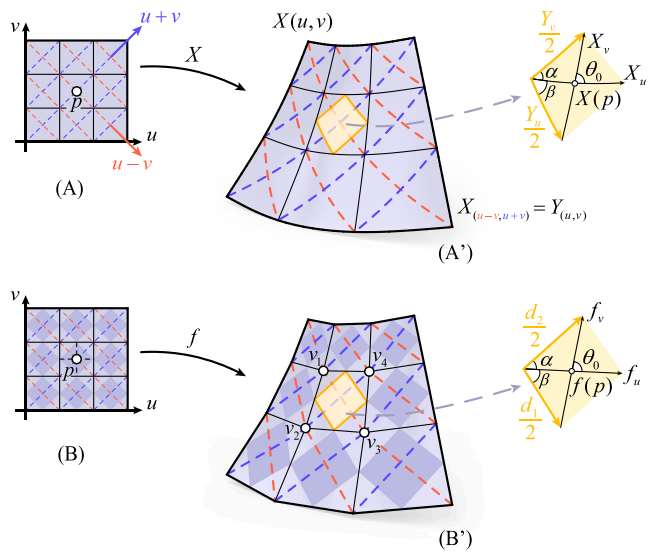

Fig. 5. Top: A smooth parametrization $\mathbf{X}(u,v)$ and its diagonal parametrization $\mathbf{Y}(u,v) = \mathbf{X}(u-v,u+v)$ form an I-web when $\frac{\|\mathbf{X}_v\|}{\|\mathbf{X}_u\|}$ and $\frac{\|\mathbf{Y}_v\|}{\|\mathbf{Y}_u\|}$ are constant. Down: Discrete derivative mapping from a regular triangulated grid as parameter domain to a triangle mesh. Discrete derivatives $\mathbf{f}_u$ and $\mathbf{f}_v$ approximate the second-order smooth derivatives, while $\mathbf{d}_1$ and $\mathbf{d}_2$ approximate the first-order smooth derivatives. These discrete derivatives have constant angles between them and form a DI-web.

Proof. Suppose there exist constant values λ and μ such that $\frac{\|\mathbf{Y}_v\|}{\|\mathbf{Y}_u\|} = \lambda$ and $\frac{\|\mathbf{X}_u\|}{\|\mathbf{X}_v\|} = \mu$. Then we have

$$\mathbf{Y}_v^2 = \lambda^2\mathbf{Y}_u^2 \Leftrightarrow (\mathbf{X}_u + \mathbf{X}_v)^2 = \lambda^2(\mathbf{X}_u - \mathbf{X}_v)^2,$$

which simplifies to $\cos\theta_0 = \frac{(1+\mu^2)(\lambda^2-1)}{2\mu(1+\lambda^2)}$, where θ_0 is the angle between $\mathbf{X}_u$ and $\mathbf{X}_v$, as shown in Fig. 5. Let θ be the angle between $\mathbf{Y}_u$ and $\mathbf{Y}_u$. Then $\cos\theta = \frac{\mu^2-1}{\sqrt{(\mu^2+1)^2-4\mu^2\cos^2\theta}}$. The expressions for $\cos\theta_0$ and $\cos\theta$ are constant and match those given in Eq. (3). Furthermore, the angles α between $\mathbf{Y}_u$ and $\mathbf{X}_u$ and β between $\mathbf{Y}_v$ and $\mathbf{X}_u$ are computed as $\cos\alpha = \frac{\mu+\cos\theta_0}{\sqrt{\mu^2+1+2\mu\cos\theta_0}}$ and $\cos\beta = \frac{\mu-\cos\theta_0}{\sqrt{\mu^2+1-2\mu\cos\theta_0}}$, which correspond to Eq. (5) after simplification, meaning that $\mathbf{Y}(u,v)$ is isogonal with respect to $\mathbf{X}(u,v)$. Specifically, when $\theta = \theta_0$, it is computed that $\lambda = \mu$, θ satisfies Eq. (8), and α and β satisfy Eq. (10).

Remark. The theorem provides only the sufficient condition for a net to be isogonal; it does not constitute a necessary condition for an I-net.

The parametrizations $\mathbf{X}(u,v)$ and $\mathbf{Y}(u,v)$ represent the same smooth surface and form a 4-web with constant angles between the four families of web curves.

Theorem 8. *A smooth parametrization $\mathbf{X}(u,v)$ and its diagonal parametrization $\mathbf{Y}(u,v) = \mathbf{X}(u-v,u+v)$ form an isogonal 4-web (I-web) if the ratios $\frac{\|\mathbf{X}_u\|}{\|\mathbf{X}_v\|}$ and $\frac{\|\mathbf{Y}_v\|}{\|\mathbf{Y}_u\|}$ are constant.*

On an infinitesimal scale, the diagonal parametrization $\frac{1}{2}\mathbf{Y}(u,v)$ is a CBP of the isogonal parametrization $\mathbf{X}(u,v)$ with similar inscribed (θ,θ_0)−parallelograms as discussed in Section 3.1.

Corollary 9. *An I-net possesses similar parallelograms in the CBP.*

Several special cases arise when specific values of λ or μ are chosen, corresponding to particular shapes of the parallelograms, as follows:

- *I-net with $\lambda = 1$.* The angle θ_0 between the partial derivatives $\mathbf{X}_u$ and $\mathbf{X}_v$ satisfies the Eq. (3), which implies that $\lambda = 1 \Leftrightarrow \theta_0 = \frac{\pi}{2}$, see Fig. 6-(A). Our proposed I-net definition is compatible with the orthogonal net, where two families of curves intersect orthogonally.

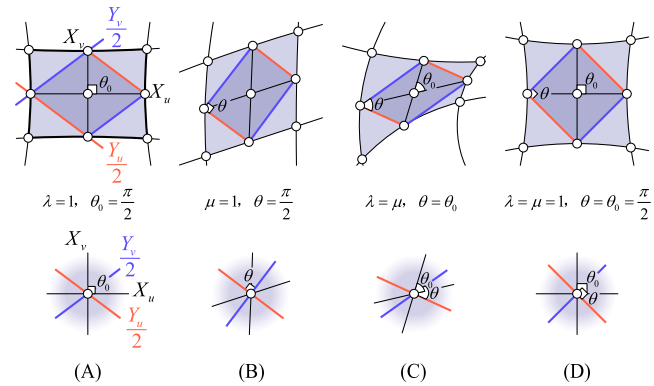

Fig. 6. Special cases for I-net and I-web based on the representation of similar parallelograms in the CBP. (A) $\lambda = 1 \Leftrightarrow \theta_0 = \frac{\pi}{2}$. I-net with similar rhombuses becomes O-net. (B) $\mu = 1 \Leftrightarrow \theta = \frac{\pi}{2}$. I-net with similar rectangles. (C) $\lambda = \mu \Leftrightarrow \theta = \theta_0$. I-net with similar θ−parallelograms. $\mathbf{X}(u,v)$ and $\mathbf{Y}(u,v)$ are aligned through rotation. (D) $\lambda = \mu = 1 \Leftrightarrow \theta = \theta = \frac{\pi}{2}$. O-net with similar squares. $\mathbf{X}(u,v)$ is locally equivalent to $\mathbf{Y}(u,v)$ after a $\frac{\pi}{4}$ rotation.

Definition 10. An I-net is an orthogonal net (*O-net*) if $\lambda = 1$.

- *I-net with $\mu = 1$.* Similarly, since the angle θ between the partial derivatives $\mathbf{Y}_u$ and $\mathbf{Y}_v$ satisfies the Eq. (3), $\mu = 1$ is equivalent to $\theta = \frac{\pi}{2}$, see Fig. 6-(B). This demonstrates that the parametrizations $\mathbf{X}(u,v)$ and $\mathbf{Y}(u,v)$ play similar roles in terms of λ,μ and their respective constant angles.
- *I-net with $\lambda = \mu$.* When the parametrization $\mathbf{X}(u,v)$ has a constant ratio $\lambda = \mu$, i.e. $\frac{\|\mathbf{X}_u\|}{\|\mathbf{X}_v\|} = \frac{\|\mathbf{X}_u+\mathbf{X}_v\|}{\|\mathbf{X}_u-\mathbf{X}_v\|}$, the angle $\theta_0 = \langle\mathbf{X}_u,\mathbf{X}_v\rangle$ between the two diagonals is equal to the interior angle $\theta = \langle\mathbf{X}_u+\mathbf{X}_v,\mathbf{X}_u-\mathbf{X}_v\rangle$ of the infinitesimal parallelograms. This can also be proven in the reverse direction. The constant angle can be computed from Eq. (8) as $\arccos(\frac{1}{2}(\lambda-\frac{1}{\lambda}))$. $\mathbf{X}(u,v)$ and $\mathbf{Y}(u,v)$ are locally aligned through rotation, see Fig. 6-(C).
- *I-net with $\lambda = \mu = 1$.* This implies $\theta = \theta_0 = \frac{\pi}{2}$. Locally, $\mathbf{X}(u,v)$ coincides with $\mathbf{Y}(u,v)$ after a rotation of $\frac{\pi}{4}$, see Fig. 6-(D).

The discussion can be extended to the discrete nets.

4.3. Discrete isogonal net and web

We generalize the discussion of I-net and I-web to their discrete counterparts. Similar results can be obtained on meshes.

Theorem 11. *Let $\mathbf{f} : \mathbb{Z}^2 \to \mathbb{R}^3$ be a quad mesh with vertices $\mathbf{v}_i, i \in \{1,2,3,4\}$ in each quad face. The discrete derivatives $\mathbf{d}_1 = \mathbf{v}_3 - \mathbf{v}_1$ and $\mathbf{d}_2 = \mathbf{v}_4 - \mathbf{v}_2$ approximate the first-order smooth derivatives, while the discrete derivatives $\mathbf{f}_u = \frac{1}{2}(\mathbf{v}_3+\mathbf{v}_4-\mathbf{v}_1-\mathbf{v}_2)$ and $\mathbf{f}_v = \frac{1}{2}(\mathbf{v}_1+\mathbf{v}_4-\mathbf{v}_2-\mathbf{v}_3)$ approximate the second-order smooth derivatives at the barycenter $\mathbf{f}(\mathbf{p})$ of each quad face, where $\mathbf{p}$ is the barycenter of each quad domain. The mesh $\mathbf{f}$ is isogonal (DI-net) if the ratios $\frac{\|\mathbf{d}_2\|}{\|\mathbf{d}_1\|}$ and $\frac{\|\mathbf{f}_u\|}{\|\mathbf{f}_v\|}$ are constant.*

Proof. As seen in Fig. 5-down, the discrete derivatives $\mathbf{v}_3 - \mathbf{v}_1$ and $\mathbf{v}_4 - \mathbf{v}_2$ are parallels to the edges of the inscribed parallelograms of the CBP, thus approximating the first-order smooth derivatives. The discrete derivative $\mathbf{f}_u$ and $\mathbf{f}_v$ can be rewritten as $\mathbf{f}_u = \frac{1}{2}[(\mathbf{v}_3-\mathbf{v}_1)-(\mathbf{v}_2-\mathbf{v}_4)]$ and $\mathbf{f}_v = \frac{1}{2}[(\mathbf{v}_4-\mathbf{v}_2)-(\mathbf{v}_3-\mathbf{v}_1)]$, thus approximating the second-order smooth derivatives. The barycenter $\mathbf{f}(\mathbf{p})$ of each quad face is also the barycenter of the inscribed parallelograms, since $\mathbf{f}(\mathbf{p}) = \mathbf{v}_1+\mathbf{v}_2+\mathbf{v}_3+\mathbf{v}_4 = \frac{1}{2}(\frac{\mathbf{v}_1+\mathbf{v}_2}{2}+\frac{\mathbf{v}_3+\mathbf{v}_4}{2}) = \frac{1}{2}(\frac{\mathbf{v}_1+\mathbf{v}_4}{2}+\frac{\mathbf{v}_2+\mathbf{v}_3}{2})$. Let $\frac{\|\mathbf{d}_2\|}{\|\mathbf{d}_1\|} = \lambda$ and $\frac{\|\mathbf{f}_u\|}{\|\mathbf{f}_v\|} = \mu$, θ and θ_0 be the angles between $\mathbf{d}_1$ and $\mathbf{d}_2$, and $\mathbf{f}_u$ and $\mathbf{f}_v$, respectively. Then

$\|\mathbf{v}_4 - \mathbf{v}_2\|^2 = \lambda^2\|\mathbf{v}_3 - \mathbf{v}_1\|^2$ and $\|(\mathbf{v}_3 - \mathbf{v}_1) - (\mathbf{v}_2 - \mathbf{v}_4)\|^2 = \mu^2\|(\mathbf{v}_4 - \mathbf{v}_2) - (\mathbf{v}_3 - \mathbf{v}_1)\|^2$ simplify to Eq. (3), which proves the lemma.

The angles between $\mathbf{f}_u$ and $\mathbf{d}_1$ and between $\mathbf{f}_v$ and $\mathbf{d}_1$ computed as Eq. (5) are constant. It indicates that quad mesh $\mathbf{f}$ and $\mathbf{d}$ form a discrete isogonal 4-web.

Theorem 12. *A quad mesh* $\mathbf{f}$ *and its diagonal quad mesh* $\mathbf{d}$ *form a discrete isogonal 4-web (DI-web) if the diagonal ratio* $\frac{\|\mathbf{d}_2\|}{\|\mathbf{d}_1\|}$ *and medial-line ratio* $\frac{\|\mathbf{f}_u\|}{\|\mathbf{f}_v\|}$ *are constant.*

Remark. The isogonal condition for a DI-web is defined at the quad faces rather than at the vertex stars. There is no direct proof that the angles between edges emanating from each vertex are constant. However, analogous to the smooth case, DI-webs are expected to exhibit nearly constant angles at the vertices.

The DI-net, along with the mesh formed by the medial lines and the two diagonal meshes, can all be viewed as discrete parametrizations of the same smooth surface.

The constant angle in a DI-net $\mathbf{f}$ is characterized by the angle θ_0 between the discrete derivative $\mathbf{f}_u$ and $\mathbf{f}_v$, which corresponds to the angle between the medial lines of the control quads and also the diagonal lines of all the inscribed (θ, θ_0)−parallelograms. The constant angle θ between the two diagonals implies that the corresponding edges of the diagonal mesh pairing have a constant ratio.

Proposition 13. *The quads of a DI-net are* (θ, θ_0)*−quads with constant values* λ *and* μ*, meaning they have similar parallelograms in the CBP.*

It is applicable for discrete analysis corresponding to the smooth theory when specific values of λ or μ are chosen, as follows:

- *DI-net with* $\lambda = 1$. All the similar parallelograms of a DI-net transform into similar rhombuses.

Definition 14. A DI-net is orthogonal (*DO-net*) if $\lambda = 1$.

Corollary 15. *A DO-net consists of similar rhombuses in the CBP.*

- *DI-net with* $\mu = 1$. The diagonal mesh pairing of a DI-net with $\mu = 1$ is orthogonal, which makes the parallelograms similar rectangles in the CBP.

Corollary 16. *A DI-net with* $\mu = 1$ *consists of similar rectangles in the CBP.*

This aligns with the discrete orthogonal net settings that appear in the diagonal direction of a control mesh [8,9,14,15].

- *DI-net with* $\lambda = \mu$. When generalized to the discrete case, all (θ, θ_0)−quads transition to θ−quads within a DI-net. The resulting DI-net exhibits a constant angle between the two medial lines and the same angle between the two diagonals of each quad, indicating that the mesh is isogonal with respect to the medial line mesh and the diagonal meshes simultaneously. These meshes discretize the same smooth surface and can be transformed by a rotation around the surface normal locally.

Corollary 17. *A DI-net with* θ*−quads possesses similar* θ*−parallelograms in the CBP. The shape of the parallelograms is determined by the constant ratio of the diagonal lengths of all quads.*

- *DI-net with* $\lambda = \mu = 1$. The parallelograms become squares, where both the ratio of the diagonal lengths and the ratio of the medial lines are equal to 1.

Corollary 18. *A DO-net with* θ*−quads consists of squares in the CBP.*

The DO-net represents a special case of the orthogonal mesh [4], where the CBP consists of rhombuses of varying shapes. When all quads are planar, the DO-net represents a discrete principal curvature net, featuring similar rhombuses, which aligns with the findings in [4]. The advantageous properties and applications of principal curvature nets can be explored in a manner analogous to previous studies.

As a discretization of an isothermic net, represented by the planar CBP with parallelograms being squares [18], the DO-net with planar $\frac{\pi}{2}$-quads serves as another representation of a discrete isothermic net. The difference between these two representations lies in the planarity constraint applied to the CBP in the former and to the control quads in the latter. However, both methods feature squares in the CBP.

5. Construction of I-nets

In this section, we explore the construction of I-nets with similar parallelograms on kinematic surfaces.

An I-net is closely related to Darboux surfaces and kinematic motions. A *Darboux surface* is generated by the movement of a curve, known as the generatrix. The parametrization $X(u, v) = (x, y, z)$ in the (u, v) parameter domain is given by:

$$[x \quad y \quad z]^T = A(v)[f(u) \quad g(u) \quad h(u)]^T + [a(v) \quad b(v) \quad c(v)]^T,$$

where A(v) is an orthogonal matrix and $(a(v), b(v), c(v))$ represents a translation.

A special class of Darboux surfaces are *kinematic surfaces* [19], where the generatrices undergo uniform smooth motions with constant speed. There are three types of kinematic surfaces: *translation surfaces*, *rotational surfaces*, and *helical surfaces*. For translation surfaces, the matrix $A(v)$ is the identity matrix I_3. For rotational and helical surfaces, $A(v)$ is a rotational matrix:

$$A(v) = \begin{bmatrix} \cos(v) & -\sin(v) & 0 \\ \sin(v) & \cos(v) & 0 \\ 0 & 0 & 1 \end{bmatrix}.$$

We begin by analyzing isometry mappings of I-nets on developable surfaces in Section 5.1. A straight line moving at a constant speed and angle relative to another forms a translation surface of congruent parallelograms. This planar translation surface can be continuously deformed into a series of developable surfaces, ultimately forming a rotational cylinder.

In Section 5.2, we delve into the conformal mappings of I-nets on rotational and helical surfaces. To facilitate the creation of I-nets, explicit isothermal representations are employed to construct I-nets on these surfaces. Notably, any I-net on a sphere can be mapped to a planar I-net via stereographic projection, where the vertices are mapped to the plane and the geometric connectivity is preserved.

Subsequently, in Section 5.3, we introduce a propagation algorithm that leverages loxodromes and parallel circles to model I-nets on general rotational surfaces.

The constructed nets serve as an effective starting point for discretization and optimization to achieve higher convergence and enable more extensive shape exploration, as discussed in Section 6.

5.1. I-nets on developable surfaces

The shear grid discussed in Section 3.3 can be seen as a translation surface produced by two straight lines moving along each other at a constant speed and a constant inclination angle. This process results in a planar I-net with congruent parallelograms, which can be bent into various shapes without stretching or tearing. The resulting surfaces are *developable surfaces*, including a general cylinder, a cone, a tangent surfaces of a space curve, or a composite shape formed by their combination.

The bending process is an isometric deformation that preserves the congruence of all inscribed parallelograms and can be implemented

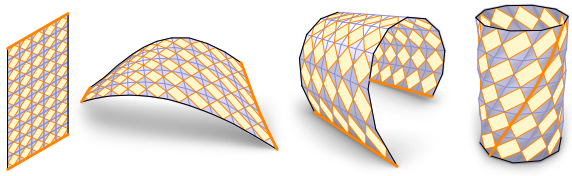

Fig. 7. I-nets on developable surfaces are isometric to each other and can be bended from a planar sheared grid with congruent parallelograms continuously to a rotational cylinder. The geodesic curve, which is a straight line in the plane, transforms into a helix on its corresponding rotational cylinder.

by modifying the control points of a chosen Bézier curve on the surface [29], such as a geodesic [30]. During shape editing, the edge lengths, interior angles, and areas of the parallelograms remain unchanged, see Fig. 7.

5.2. I-nets from isothermal parametrizations

A regular surface of revolution can be parametrized by two general parameters u and v as

$$S(u,v) = (f(v)\cos u, f(v)\sin u, g(v)), \tag{14}$$

where $f(v)$ and $g(v)$ determine the shape of the surface of revolution by describing the radius and height of the surface as functions of the parameter v.

This parametrization represents geodesic parallel coordinates [29], where profile curves $S(u = const, v)$ are geodesic orthogonal to the parallels $S(u, v = const)$, implying $F = 0$ in the first fundamental form.

When $E = f^2(v) = f'^2(v) + g'^2(v) = G$, $S(u,v)$ is an *isothermal* parametrization, where $E = G$ and $F = 0$. An *isothermic net* is characterized by isothermal parametrization. Any two regular surfaces are locally conformal, as established by the existence of isothermal coordinate systems on any regular surface. These systems enable a surface to be locally conformal to a plane, and by composition, locally conformal to any other surface, as cited in [31].

A sheared grid with regular spacing can be isometrically mapped onto a rotational cylinder, preserving quad spacing and shape, as seen in Fig. 7. However, only a conformal mapping exists between a planar patch and a general surface of revolution, which alters quad spacing.

An isothermal parametrization maps small squares in the (u,v) domain to small squares on the surface, preserving angles between curves. In this case, $\theta = \theta_0 = \frac{\pi}{2}$ and $\lambda = \mu = 1$, making both the control net and its diagonal net O-nets. Furthermore, an I-net with angles of $\frac{\pi}{4}$ or $\frac{3\pi}{4}$ can be obtained by selecting one family of its diagonal isolines, which are *loxodromes* as discussed in Section 5.3, and one family of isolines. Each $(\theta, \theta_0 = \frac{\pi}{4})$–quad of the I-net is conformally mapped from a parallelogram formed by two neighboring squares in the (u,v) domain. The mid-edge subdivided parallelogram of this parallelogram can be computed with $(\theta, \theta_0) = (\arccos\frac{1}{\sqrt{5}}, \frac{\pi}{4})$ and $(\lambda, \mu) = (\sqrt{5}, \sqrt{2})$, see Fig. 8.

Explicit isothermal parametrizations can be obtained by choosing different functions $f(v)$ and $g(v)$ for some common surfaces of revolution, as given by Eq. (14):

- Cylinder: $f(v) = r, g(v) = rv$
- Sphere: $f(v) = r\,\mathrm{sech}\, v, g(v) = r\tanh v$
- Catenoid: $f(v) = r\cosh v, g(v) = rv$

where r is a constant.

Another common isothermal parametrization is for the helicoid, where g in Eq. (14) is a function of u, that is

- Helicoid: $f(v) = r\sinh v, g(u) = ru$.

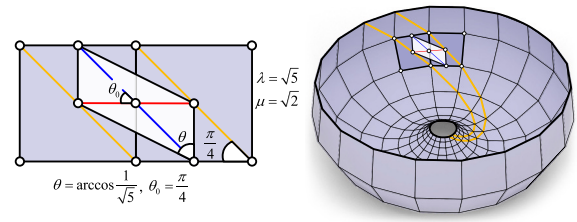

Fig. 8. Left: Two parallel diagonals and two parallel edges of two neighboring squares form a parallelogram, whose mid-edge subdivided parallelogram has $(\theta, \theta_0) = (\arccos\frac{1}{\sqrt{5}}, \frac{\pi}{4})$ and $(\lambda, \mu) = (\sqrt{5}, \sqrt{2})$. Right: I-net characterized by these similar parallelograms can be generated from an isothermal net.

Combining the catenoid $\bar{C}$ and the helicoid $\bar{H}$, a family of conjugate minimal surfaces can be produced with a changing parameter t:

- Conjugate minimal surface: $(\cos t)\bar{C} + (\sin t)\bar{H}$ for $t \in \mathbb{R}$.

I-nets with similar inscribed parallelograms can be generated on these five kinds of surfaces, where the angles are $(\theta, \theta_0) = (\arccos\frac{1}{\sqrt{5}}, \frac{\pi}{4})$, as shown in the Fig. 9-$(A_1 - E_1)$. In Fig. 9-$(A_3 - E_3)$, applying Möbius transformations [27] to the prescribed I-net yields a variety of new surface shapes, which aids in shape exploration and serves as good initializations for further optimization with different constant angles.

From the smooth I-net, we sample the curve network at discrete points, typically at intersections. These points are then connected to form edges and faces, constructing the discrete I-net. The resulting mesh provides an effective initialization for optimizing I-nets with other constant angles, as shown in Fig. 9-$(A_1 - E_1)$ and -$(A_3 - E_3)$. Fig. 9-$(A_2 - E_2)$ and -$(A_4 - E_4)$ illustrate the optimized I-nets with specific angles gliding along the corresponding surfaces depicted in Fig. 9-$(A_1 - E_1)$ and -$(A_3 - E_3)$, respectively. The optimization process is detailed in Section 6.

Any two regular surfaces are locally conformal [31], a property that facilitates the construction of various isothermal parametrizations through conformal mappings, such as Möbius transformations [27]. Consequently, given an isothermal parametrization, I-nets with similar inscribed parallelograms characterized by angles $(\arccos\frac{1}{\sqrt{5}}, \frac{\pi}{4})$ can be obtained either via conformal transformations or generated from isothermic nets after such transformations. Specifically, isometry, as a special conformal mapping, preserves all the inscribed parallelograms of quads on an infinitesimal scale [11,14,15] and the Gaussian curvatures. The method is well-suited for the paneling of freeform architectural facades using bendable materials such as plastic, wooden or metal sheets, as demonstrated in studies [10,11,15] and others.

Stereographic projection. Stereographic projection is a conformal map from a sphere to a plane.

A sphere S^2 without the north pole $N = (0,0,1)$ can be mapped conformally to a plane under the stereographic projection [31], which projects points on the sphere from N to the plane while preserving geometric connectivity. Thus, an I-net with similar parallelograms on a sphere can be mapped to a planar one while preserving the angles, see Fig. 10.

5.3. I-nets formed by loxodromes and parallels

We represent the parametrization in Eq. (14) as $S(\alpha, s) = (f(s)\cos\alpha, f(s)\sin\alpha, g(s))$ using the arc-length parameter s and the angle $\alpha \in [0, 2\pi)$. The parametrized curve $(f(s), 0, g(s))$ represents the profile curve, also known as the *meridian*. For a fixed s_i, $S(\alpha, s_i)$ describes a parallel circle, referred to as a *parallel*.

On a surface of revolution, there exist two families of special curves that intersect the meridians at a constant angle γ; these curves are

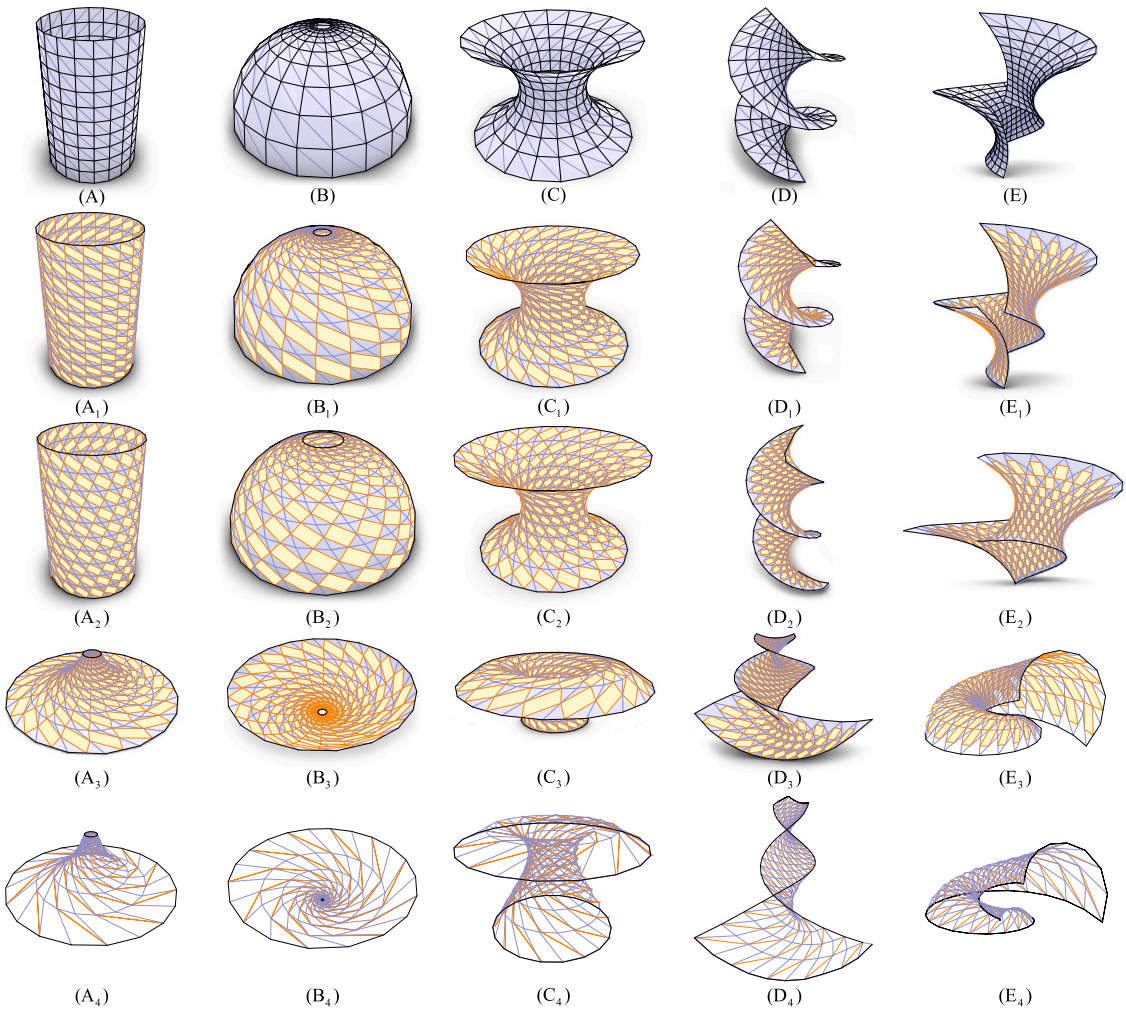

Fig. 9. $(A_1 - E_1)$ I-nets with similar inscribed parallelograms, characterized by angles $(\theta, \theta_0) = (\arccos \frac{1}{\sqrt{5}}, \frac{\pi}{4})$ can be extracted from the isothermal parametrization on surfaces. Examples include (A) a cylinder, (B) a sphere, (C) a catenoid, (D) a helicoid, and (E) a conjugate minimal surface combined by catenoid and helicoid. These I-nets can be further optimized to have $(\theta, \theta_0) = \left(\frac{4\pi}{9}, \frac{\pi}{4}\right)$ in $(A_2 - E_2)$, approximating the corresponding surfaces. Alternatively, they can be transformed conformally under Möbius transformations to new surface shapes in $(A_3 - E_3)$, and then optimized to have $\theta = \theta_0 = \frac{5\pi}{18}$ approximated on the surfaces in $(A_4 - E_4)$. The Hausdorff distances between the meshes in $(A_4 - E_4)$ and the underlying subdivided meshes in $(A_3 - E_3)$ are $1.959, 0.016, 38.593, 3.120$ and 9.464, respectively, relative to their corresponding diagonal lengths of the bounding boxes.

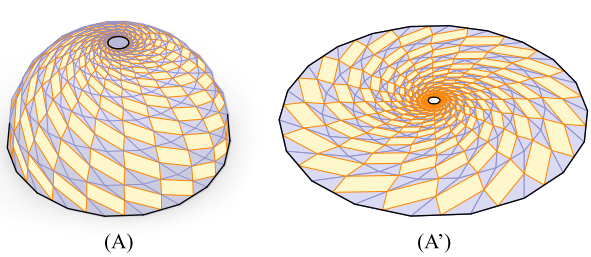

Fig. 10. (A) From Fig. 9-(B), an I-net with similar parallelograms covers part of a unit sphere. (A') Under stereographic projection, it is mapped to the plane, preserving the angles of all similar parallelograms.

symmetric with respect to the meridians and are called *loxodromes*. The net formed by these two families of loxodromes is an I-net characterized by $(\theta, \theta_0) = (\frac{\pi}{2}, 2\gamma)$–parallelograms, which are essentially similar rectangles.

Since the meridians and parallel circles form the principal curvature lines of the surface of revolution, the angle between the meridians and parallel circles is $\frac{\pi}{2}$. Consequently, the angle between a family of loxodromes and all the parallel circles is $\theta_0 = \frac{\pi}{2} - \gamma$. Thus, this family of loxodromes and parallel circles form an I-net with a constant angle θ_0, but may have different interior angle θ for the inscribed parallelogram.

Remark. The isothermal nets discussed in Section 5.2 are special principal curvature nets, and their diagonals are two families of loxodromes with $\theta_0 = \frac{\pi}{4}$ and $\theta_0 = \frac{3\pi}{4}$.

Specifically, the helices and logarithmic spirals are loxodromes of the rotational cylinder and cone, respectively. These curves are also known as *curves of constant slope* [32], as they maintain a constant angle with respect to unchanged planes. A helix given by $(\cos(as), \sin(as), bs)$ on a cylinder $S(u, v) = (\cos u, \sin u, v)$ maintains a constant angle with respect to the parallels. As seen in Fig. 9, a helix on the cylinder is highlighted. A rotational cone with a cone vertex angle of 2γ can be parametrized as $S(u, v) = (u \sin\gamma \cos v, u \sin\gamma \sin v, u \cos\gamma)$ with $0 < u$ and $0 < v < 2\pi$. There exist logarithmic spiral curves $S(ce^{v \sin\gamma \tan\theta_0}, v)$ with a constant c that intersect the parallel circles at a constant angle θ_0. Consequently, I-nets on rotational cylinders and cones can be constructed by a family of parallel circles and a family of helices or logarithmic spirals, respectively.

Any loxodrome on a general rotational surface can be explicitly parameterized by an arc-length parameter s as [33]

$$l(s, k) = S(\alpha(s, k), t(s)), \tag{15}$$

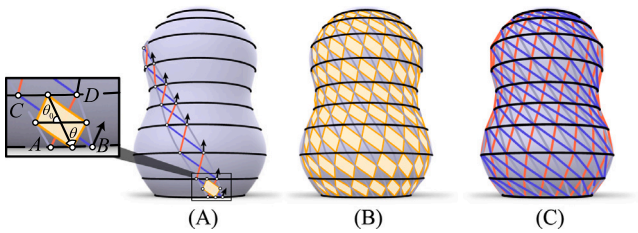

Fig. 11. On a general surface of revolution, an I-web is constructed using three families of loxodromes and the parallel circles. (A) The process begins with two neighboring loxodromes that form a constant angle $\frac{\pi}{2}-\theta_0$ with the meridians and intersect a parallel circle at points A and B. Two neighboring points C and D on the loxodromes are computed to satisfy Eq. (16). Subsequently, a strip of quads with similar inscribed (θ,θ_0)−parallelograms is modeled using the propagation algorithm outlined in Alg. 1. By uniformly rotating around the axis, an I-net covering the rotational surface with congruent strips is constructed and its discretization can be extracted in (B). (C) The two families of diagonal curves create non-trivial isogonal curve patterns and are also loxodromes with angles related to λ and μ. Loxodromes and parallel circles form an isogonal 4-web. Multiple I-nets with different similar parallelograms can be extracted.

where $t(s) = s\sin\theta_0 + c, \alpha(s,k) = \cos\theta_0 \int_k^t \frac{d\xi}{f(t(\xi))}$ for constant c, k and $\theta_0 \in [0,\pi]$. Two neighboring loxodromes $l(s,k_j)$ and $l(s,k_{j+1})$ intersect two neighboring parallel circles $S(\alpha_i,t)$ and $S(\alpha_{i+1},t)$ at four points $A = S(\alpha(s_i,k_j),t_i)$ and $B = S(\alpha(s_i,k_{j+1}),t_i)$ on $S(\alpha,t_i)$ with computed $s_i = \frac{t_i-c}{\sin\theta_0}$, and $C = S(\alpha(s_{i+1},k_j),t_{i+1})$ and $D = S(\alpha(s_{i+1},k_{j+1}),t_{i+1})$ on $S(\alpha,t_{i+1})$ with computed $s_{i+1} = \frac{t_{i+1}-c}{\sin\theta_0}$. On an infinitesimal scale, points A,B,C,D form a planar (θ,θ_0)-quad and its mid-edge subdivided parallelogram lies on the surface. The straight diagonal and medial-line distances measured in the ambient space can be considered as the geodesic distances on the surface. The angles θ and θ_0 of the inscribed parallelogram are determined by edge ratios λ and μ, which are given in Eq. (3). The ratios can be expressed as

$$\lambda = \frac{\|D-A\|}{\|B-C\|}, \mu = \frac{\|B+D-A-C\|}{\|C+D-A-B\|}. \tag{16}$$

A family of parallel circles with parameters $s_0, s_1, \dots, s_m$ and a family of loxodromes with parameters $k_0, k_1, \dots, k_n$ form an I-net with a grid of points, where the integers m and n represent the number of quads in the horizontal and vertical directions, respectively. When all the quads satisfy Eq. (16), the isogonal parametrization on the surface of revolution have similar inscribed parallelograms, and its diagonal parametrization is isogonal with constant angle θ. However, this parametrization involving the solution of s_i (for $i = 0,1,\dots,m$) and k_j (for $j = 0,1,\dots,n$) from Eq. (16) is not directly solved and explicitly represented.

A direct method for constructing an I-net with given angles (θ,θ_0) for similar inscribed parallelograms on a surface of revolution involves using the propagation method, as described in Alg. 1 in Appendix A.3. This method begins by selecting a loxodrome and a parallel circle with two points. New points are then added incrementally to form a strip composed of (θ,θ_0)−parallelograms, see Fig. 11-(A). The I-net covering the surface is then generated by rotating this strip at a constant speed, see Fig. 11-(B). This approach allows users to freely choose the net's constant angles (θ,θ_0), as well as its spacing and density.

The resulting I-net can be further utilized to construct an I-web and other I-nets on the same surface. The two families of diagonal curves of the I-net are also loxodromes, as they form constant angles with the parallels. Consequently, an isogonal web composed of three families of loxodromes and a family of parallel circles (which are also loxodromes with an angle of $\frac{\pi}{2}$ relative to the meridian) can be produced on the surface of revolution, as shown in Fig. 11-(C). Multiple non-trivial I-nets can be extracted from any two families of loxodromes, including their reflections with respect to the meridian planes.

Remark. A special case of the I-nets discussed above occurs when $\theta = \theta_0$. In this scenario, the spacing quality of the resulting net is highly dependent on the curvature changes of the rotational surface.

6. Computational design of DI-nets

The computational design of DI-nets involves several key steps: expressing non-linear geometric constraints associated with mesh vertices, initializing the system, iteratively optimizing to satisfy these constraints, or enabling interactive design.

The *Guided Projection* algorithm, introduced in [22], is employed for the computational design tasks. This algorithm is a Gauss–Newton method that approximates the function using a first-order Taylor expansion and iteratively updates the parameters to minimize the sum of squared residuals. It necessitates that the equation representations be quadratic or lower in degree, meaning the equations must be transformed to have a maximum degree of 2. Subsequently, all local constraints are integrated across the entire mesh as energy terms, iteratively refining the mesh parameters until both a satisfactory appearance and convergence are achieved.

6.1. Geometry constraints

The geometry constraint expressions for DI-nets with similar parallelograms are essential for preserving the geometric properties of the nets and are integrated into the target function for optimization.

6.1.1. DI-net with (θ,θ_0)−parallelograms

Constraints of (θ,θ_0)−quads. Within a (θ,θ_0)−quad with four vertices $\mathbf{v}_i^f, (i = 1,\dots,4)$, the two diagonal vectors are $\mathbf{d}_1 = \mathbf{v}_3^f - \mathbf{v}_1^f$ and $\mathbf{d}_2 = \mathbf{v}_4^f - \mathbf{v}_2^f$ and the two medial-line vectors are $\mathbf{m}_{13} = \frac{1}{2}(\mathbf{v}_3^f + \mathbf{v}_4^f - \mathbf{v}_1^f - \mathbf{v}_2^f)$ and $\mathbf{m}_{24} = \frac{1}{2}(\mathbf{v}_1^f + \mathbf{v}_4^f - \mathbf{v}_2^f - \mathbf{v}_3^f)$. A constant ratio λ between the two diagonal lengths and a constant ratio μ between the two medial-line lengths of all quads ensure the similarity of all inserted parallelograms. From Proposition 4, the constraints for λ and μ apply to each quad face $f, (f = 1,\dots,|F|)$ satisfy Eqs. (11), (12), which are equivalent to

$$\text{Eq. (11)} \Leftrightarrow \begin{cases} (\mathbf{v}_3^f - \mathbf{v}_1^f)^2 = L^a, \\ (\mathbf{v}_4^f - \mathbf{v}_2^f)^2 = L^b, \\ L^b = c_1 L^a, \\ \lambda^2 = c_1, \end{cases} \tag{17}$$

$$\text{Eq. (12)} \Leftrightarrow \begin{cases} (\mathbf{v}_3^f + \mathbf{v}_4^f - \mathbf{v}_1^f - \mathbf{v}_2^f)^2 = L^p, \\ (\mathbf{v}_1^f + \mathbf{v}_4^f - \mathbf{v}_2^f - \mathbf{v}_3^f)^2 = L^q, \\ L^q = c_2 L^p, \\ \mu^2 = c_2, \end{cases} \tag{18}$$

Here L^a, L^b, L^p, L^q, c_1 and c_2 are auxiliary variables ensuring that the equation representations are at most quadratic, thus compatible with the algorithm in [22].

The variables $\mathbf{v}_i^f, L^a, L^b, L^p, L^q, c_1$ and c_2 vary across each quad faces of the mesh, whereas the variables λ and μ remain constant and can be assigned specified values λ_0 and μ_0 as required.

Given ratios constraints. Similar parallelograms with given ratios λ_0 and μ_0 are enforced by the constraints:

$$\lambda - \lambda_0 = 0, \quad \mu - \mu_0 = 0, \tag{19}$$

which regulate the shape of all the parallelograms. Special cases include $\lambda_0 = 1$ or $\mu_0 = 1$.

Given angles constraints. Since the angles θ and θ_0 are functions of λ and μ as given by Eq. (3), the shape of all the parallelograms, which is subject to the isogonal condition, can be controlled by specifying constant angles $\bar{\theta}$ and $\bar{\theta}_0$. The relationships are as follows:

$$\begin{cases} (1+c_1)(c_2-1) = 2\cos\bar{\theta} \cdot \lambda(1+c_2), \\ (1+c_2)(c_1-1) = 2\cos\bar{\theta}_0 \cdot \mu(1+c_1), \end{cases} \tag{20}$$

which are quadratic equations since $\cos\bar{\theta}$ and $\cos\bar{\theta}_0$ are computed as constant values.

A DI-net composed of $(\theta,\theta_0)-$quads is constrained by Eqs. (17), (18), which correspond to the energy term $E_\square$. Eqs. (19), (20) are selected based on the user specifications and correspond to energy term E_*.

6.1.2. DI-net with θ_0-parallelograms

Although $\theta = \theta_0$ condition imposes additional restrictions by requiring both the isogonal medial-line mesh and the isogonal diagonal meshes, the equivalent condition specified by Eq. (13) is simpler when applied to each quad than when either condition is considered individually.

Eq. (13) is a quadratic equation in terms of mesh vertices as variables, which is compatible with standard Gauss–Newton methods for optimization. This formulation offers significant advantages in simplifying the constraints and implementing the optimization process, particularly when compared to the isogonal condition defined by two unit tangent vectors along two discrete curves at vertices [9–11,16,17], along two diagonals [8,9,14,15] or along two medial lines [9]. Moreover, this isogonal condition provides additional degrees of freedom for the mesh, enabling it to accommodate a wider range of constraints tailored for various curve nets, similar to the discussion in [4].

Constraints of $\theta-$quads. $\theta-$Quads are special case of $(\theta,\theta_0)-$quads where $\theta = \theta_0$ or equivalently $\lambda = \mu$. The constraints can be implemented based on the aforementioned conditions and further reinforced by setting $\lambda = \mu$. However, the equation representations can be simplified as discussed in Proposition 6. Specifically, the condition for two diagonal vectors within a $\theta-$quad, as characterized by Eq. (13), is equivalent to

$$(\mathbf{v}_4^f - \mathbf{v}_2^f)^2 - (\mathbf{v}_3^f - \mathbf{v}_1^f)^2 - 2(\mathbf{v}_4^f - \mathbf{v}_2^f)(\mathbf{v}_3^f - \mathbf{v}_1^f) = 0. \tag{21}$$

An isogonal quad mesh composed of $\theta-$quads features similar inscribed $\theta-$parallelograms in the CBP, with their similarity controlled by a constant ratio λ between the two diagonal lengths of all quads. The ratio λ satisfy Eq. (17).

Given angle θ constraints. The shape of the $\theta-$parallelogram inscribed in the $\theta-$quad is determined by the constant angle θ or equivalently the ratio λ. $\theta-$Quads with a specified λ_0 can be enforced according to the representation given in Eq. (19). Given $\bar{\theta}_0$, the ratio λ that satisfies Eq. (8) is equivalent to

$$\lambda = \cos\bar{\theta}_0 + \sqrt{1+\cos^2\bar{\theta}_0}, \tag{22}$$

which is a linear equation since $\cos\bar{\theta}_0$ is constant.

A DI-net composed of $\theta-$quads is constrained by Eqs. (17), (21), which correspond to the energy term $E_\square$. Eqs. (19), (22) are utilized when necessary and correspond to energy term E_*.

6.2. Initialization

The quality of the initial mesh significantly impacts the efficiency of our optimization process. A good initialization for DI-nets means that the starting quad mesh contains inscribed parallelograms that are as similar as possible. Examples include DI-nets derived from planar sheared grids through conformal mapping or isometric deformation in Sections 3.3 and 5.1, DI-nets extracted from isothermal parametrizations in Section 5.2, and DI-nets formed by loxodromes and parallels on rotational surfaces in Section 5.3. Once initialized, DI-nets with modified constant angles can be optimized on the underlying surface by incorporating a surface approximation constraint, as shown in Fig. 9.

Meshes with constant angles between their unit polyline tangents—computed from three consecutive vertices at vertices [9–11,16,17], between their quad diagonals along two diagonal directions [8,9,14,15] or between two medial lines defined at faces [9] can be used for DI-net optimization. These meshes exhibit (nearly) constant angles θ or θ_0, making them suitable for constructing and optimizing DI-nets with similar parallelograms.

Orthogonal meshes are ideal for constructing orthogonal nets (O-nets), and we prefer three types: (1) meshes where orthogonality is defined by a constant angle between quad medial lines ($\lambda = 1$) [4]; (2) meshes where orthogonality is defined by a constant angle between diagonal lines ($\mu = 1$) [8,9,14,15]; and (3) meshes composed of squares with both $\lambda = \mu = 1$ [18]. Starting from these meshes, DI-nets can be efficiently optimized by gradually assigning different constant angles to achieve the desired target angles.

6.3. Optimization

Fairness constraints. They are commonly used to control the curvature quality of mesh polylines. By optimizing the spacing and aesthetic appearance of quad meshes, they ensure smoothness along polylines. The fairness term E_{fair} is defined on three consecutive vertices $\mathbf{v}_{il}, \mathbf{v}_i, \mathbf{v}_{ir}$ as:

$$E_{fair} = \sum_{i\in polyline} (2\mathbf{v}_i - \mathbf{v}_{il} - \mathbf{v}_{ir})^2.$$

Self-closeness constraints. The shape change during optimization is controlled by limiting the movement of mesh vertices between iterations, known as self-closeness. The corresponding energy term is:

$$E_{clos} = \sum_{i\in vertices} (\mathbf{v}_i - \bar{\mathbf{v}}_i)^2.$$

Vertices $\bar{\mathbf{v}}_i$ are derived from the previous iteration of $\mathbf{v}_i$.

Approximation constraints. To ensure a net gliding along a surface closely approximates it, each vertex $\mathbf{v}_i$ is constrained to lie on the surface, with the vector from $\mathbf{v}_i$ to the closest point $\mathbf{p}_i$ being orthogonal to the surface normal $\mathbf{n}_i$ at $\mathbf{p}_i$. The corresponding energy term is

$$E_{app} = \sum_{i\in vertices} ((\mathbf{v}_i - \mathbf{p}_i)\cdot\mathbf{n}_i)^2.$$

Here, the surface or mesh itself serves as a reference to control shape changes during optimization.

Boundary-gliding constraints. To maintain the quality of the mesh boundary, boundary-gliding constraints are added:

$$E_{bdry} = \sum_{i\in boundary} (((\mathbf{v}_i - \mathbf{p}_i)\cdot\mathbf{e}_{i2})^2 + ((\mathbf{v}_i - \mathbf{p}_i)\cdot\mathbf{e}_{i3})^2),$$

where $(\mathbf{e}_{i1}, \mathbf{e}_{i2}, \mathbf{e}_{i3})$ is the Frenet frame at the closest boundary point $\mathbf{p}_i$ of the reference mesh to the optimized mesh boundary point $\mathbf{v}_i$. This ensures that the vector $\mathbf{v}_i - \mathbf{p}_i$ aligns with the reference boundary tangent, which is equivalent to

$$E_{bdry} = \sum_{i\in boundary} ((\mathbf{v}_i - \mathbf{p}_i)\times\mathbf{e}_{i1})^2.$$

Target function. The target function for a DI-net is formulated by integrating local constraints across the mesh and combining them with fairness, self-closeness, approximation, and boundary-gliding terms. It is expressed as:

$$E_+ = E_\square + \omega_1 E_* + \omega_2 E_{fair} + \omega_3 E_{clos} + \omega_4 E_{app} + \omega_5 E_{bdry}.$$

Here, $E_\square$ represents the DI-net energy term, E_* represents user-defined constraints with ω_1 being 0 or 1. Typically, the weight ω_2 ranges from 0.0005 to 0.01 to influence the quality of the mesh polylines, while the weights ω_3 and ω_4 range from 0.001 to 0.1 to moderately affect the shape changes. Weight ω_5 is used in Fig. 12 and set to 0.01. A larger ω_2 value makes the mesh polylines straighten and shrink more quickly, while larger $\omega_3 - \omega_5$ values slow the changes of the mesh and the optimization process. Balancing ω_2–ω_5 is crucial for optimal results.

The optimization minimizes E_+ to achieve the desired appearance with low convergence residuals, typically requiring 10 to 30 iterations. The effectiveness of our method is demonstrated through applications on freeform surfaces, as shown in Figs. 12, 13. Detailed numerical results are provided in Table 1.

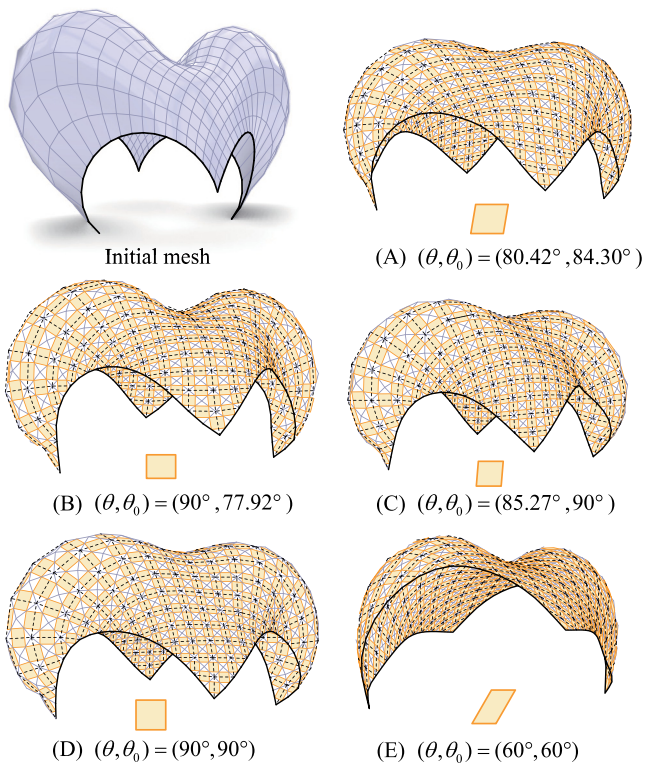

Fig. 12. Starting from a general patch, various freeform shapes are designed and covered by I-webs and similar parallelograms. (A) Direct optimization of the initial mesh to an isogonal net results in a general DI-net with similar parallelograms. (B–E) The optimized DI-nets with prescribed angles θ or θ_0 lead to special cases of inscribed parallelograms: (B) rectangles, (C) rhombuses, (D) squares, and (E) parallelograms with $\theta=\theta_0=\frac{\pi}{3}$. Computational details are provided in Table 1.

7. Conclusion

This paper presents a novel method for constructing isogonal nets (I-nets) and isogonal 4-webs (I-webs) using the checkerboard pattern method. By defining I-nets through similar mid-edge subdivided parallelograms, our approach generalizes orthogonal nets [4] and allows for constant angles between curve families that are not restricted to 90 degrees. This expands the scope of geometric design possibilities for regular surface parametrization and ensures compatibility with orthogonal nets through special cases like rhombuses, rectangles, and squares.

Our method focuses on constraining edge ratios to control angles rather than directly representing angles, yielding a simple and versatile representation that seamlessly integrates into mesh optimization algorithms. This approach simplifies the construction of I-nets and enables the creation of I-webs, extending their applications to more complex and freeform shapes. Through conformal mapping and numerical optimization, we demonstrate the versatility of I-nets and I-webs in various freeform shapes, enhancing both the aesthetic and functional qualities of surface designs. Experiments on different surfaces validate the effectiveness of our approach, highlighting its potential for both theoretical advancements and practical applications.

Overall, this work lays the foundation for new research directions and applications in geometry processing and computer-aided design. Future research will delve into further generalizations of I-nets and their integration with other specialized nets. Potential applications include paneling design for freeform architectural surfaces, gridshell structures with uniform knots [34], repetitive pattern design [35–37], auxetic quads with similar elements [38], periodic structures in additive manufacturing [39], woven fabrics with regular patterns [40], and other emerging fields.

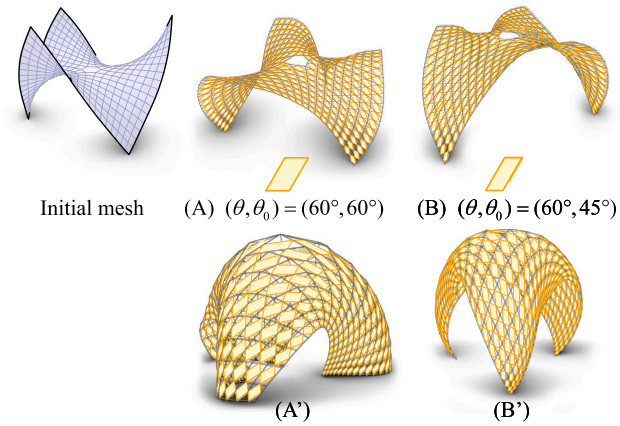

Fig. 13. A quad mesh with a singular face at the center is optimized to (A) a DI-net with $\theta=\theta_0=\frac{\pi}{3}$ and (B) a DI-net with $(\theta,\theta_0)=(\frac{\pi}{3},\frac{\pi}{4})$, respectively. (A'–B') show their corresponding Möbius transformations, preserving the geometric connectivity.

CRediT authorship contribution statement

Hui Wang: Writing – review & editing, Writing – original draft, Visualization, Validation, Software, Project administration, Methodology, Conceptualization. **Xinye Li:** Validation. **Zhi Li:** Visualization. **Cheng Wang:** Validation.

Declaration of competing interest

The authors declare that they have no known competing financial interests or personal relationships that could have appeared to influence the work reported in this paper.

Acknowledgments

The authors express gratitude to the anonymous reviewers for their valuable feedback. This work was supported by the Xi'an Jiaotong University Young Talent Support Program, China (No. 11303225010702). Zhi Li was supported by the Australian Research Council, Australia (No. FL190100014). Cheng Wang was supported by the University of East Anglia Internal Research Fund, United Kingdom (No. 60002351FA1).

Appendix

A.1. Proof of Eqs. (7)–(10)

Proof. In parallelogram $ABDC$ in Fig. 1, triangle $\triangle ABD$ and triangle $\triangle ODC$ are similar due to $\theta=\theta_0$. Consequently, we find that $p=\sqrt{2}, q=\sqrt{2}\lambda$ and $\mu=q:p=\lambda$. The relationship between the interior angle θ and the edge ratio λ, derived from Eq. (3), can be calculated as $\cos\theta=\frac{\lambda^2-1}{2\lambda}=\frac{1}{2}(\lambda-\frac{1}{\lambda})$, which indicates that θ is a function of λ, denoted as $\theta(\lambda)$. The range of λ satisfies $\sqrt{2}-1<\lambda<\sqrt{2}+1$. Substituting $q=\sqrt{2}\lambda$ into Eq. (5), we can compute $\cos\alpha$ and $\cos\beta$ as given.

A.2. Conformal mappings of planar sheared grids

Consider a sheared grid with two families of straight lines in the complex plane. The first family, denoted as C_1, consists of lines in the upper half-plane parallel to the real axis. These lines can be represented in the complex function form as:

$$C_1=\{z=t+i\mathcal{A}, \frac{\mathcal{A}}{h}\subseteq\mathbb{Z}^+, h\in\mathbb{R}^+\},$$

where t is a real variable, and $\mathcal{A}$ is a set of positive numbers with a given common difference of h. The second family, denoted as C_2, consists of lines with an inclination angle θ_0 with respect to the positive real axis. These lines can be represented as

$$C_2 = \{z = t + \mathcal{B} + i(kt), k = \tan\theta \in \mathbb{R}, \mathcal{B} \subseteq \mathbb{Z}, 0 \notin \mathcal{B}\},$$

where $k > 0$ is a real number of given $\tan\theta$ and $\mathcal{B}$ is a set of integers with a common difference of 1. These two families of lines form a sheared grid M_0 with congruent (θ_0, θ)−parallelograms, each having an interior angle θ_0 and a diagonal angle θ, and one horizontal edge length equal to 1, as seen in Fig. 3-(A).

The common difference h provides the flexibility to determine the angles θ_0 and θ, and consequently, to shape the grid M_0. When the (θ_0, θ)−parallelograms become θ−parallelograms, then the other edge length of each parallelogram is determined as $\lambda = \cos\theta + \sqrt{1 + \cos\theta^2}$. Furthermore, the real constant h can be calculated as $h = \lambda \sin\theta$. The subsequent discussion will focus on the results obtained for grid M_0 with similar θ−parallelograms under conformal mappings.

The following list provides examples of choosing two different conformal mappings.

- Let $\omega = \frac{1}{z}$. This inversion mapping is a simple *Möbius* transformation and analytic in the complex plane except at $z = 0$. ω maps the curves in C_1 to $\{z = u + iv = \frac{t}{t^2+\mathcal{A}^2} - i\frac{\mathcal{A}}{t^2+\mathcal{A}^2}\}$, which represents a family of circles given by

  $$u^2 + (v + \frac{1}{2\mathcal{A}})^2 = \frac{1}{4\mathcal{A}^2}.$$

  Additionally, it maps the curves in C_2 to $\{z = u + iv = \frac{t+\mathcal{B}}{(1+k^2)t^2+2\mathcal{B}t+\mathcal{B}^2} - i\frac{kt}{(1+k^2)t^2+2\mathcal{B}t+\mathcal{B}^2}\}$, which represents a family of circles given by

  $$(u - \frac{1}{2\mathcal{B}})^2 + (v - \frac{1}{2k\mathcal{B}})^2 = \frac{1+k^2}{4k^2\mathcal{B}^2},$$

  as shown in Fig. 3-(A').
- Let $\omega' = z^2$. This conformal mapping is analytic in the complex plane and transforms the curves in C_1 to $\{z = u + iv = t^2 - \mathcal{A}^2 + i(2\mathcal{A}t)\}$, which represents a family of confocal parabolas given by the equation

  $$v^2 - 4\mathcal{A}^2 u - 4\mathcal{A}^4 = 0.$$

  It also transforms the curves in C_2 to $\{z = u + iv = (1 - k^2)t^2 + 2\mathcal{B}t + \mathcal{B}^2 + i(2kt^2 + 2k\mathcal{B}t)\}$, where u and v satisfy the equation

  $$4k^2u^2 + (k^2 - 1)^2v^2 + 4k(k^2 - 1)uv +$$
  $$4k^2\mathcal{B}^2(k^2 - 1)u - 8k^3\mathcal{B}^2v - 4k^4\mathcal{B}^4 = 0.$$

  Since the discriminant Δ of the conic section from the given equation is $\Delta = 0$, the conic section is a parabola for all values of k. Curvilinear nets formed by parabolas for $k = \tan\frac{\pi}{4} = 1$ and $k = \tan\frac{\pi}{3} = \sqrt{3}$ are shown in Fig. 3-(B',C').

A.3. Algorithm to construct an I-web on a rotational surface

Remark. Alg. 1 enables the construction of smooth I-nets using geodesic distances on the surface. It can be extended to handle discrete correspondences by using straight-line distances in the ambient space.

A.4. Optimization statistics

See Table 1.

Data availability

Data will be made available on request.

Algorithm 1 Construct an I-web on a Rotational Surface

Input: A rotational surface with the Z−axis as the rotational axis, and constant angles (θ, θ_0).
Select a parallel circle c_0 with center $(0, 0, z_0)$ and radius r_0;
Set a point A on c_0;
Set the interval number m of quads in the horizontal direction and n of quads in the vertical direction;
Compute a loxodrome l_A with angle $\frac{\pi}{2} - \theta_0$ relative to a meridian passing through point A using Eq. (15);
Rotate l_A by $\frac{2\pi}{m}$ to obtain another loxodrome l_B that intersects c_0 at B;
Set a reasonable diagonal ratio λ;
while $i \le n$ and c_i is within the surface **do**
  Find the parallel circle c_i with center $(0, 0, z_i)$ and radius r_i, such that it intersects l_A and l_B at two points $C = (x_C, y_C, z_i) \in l_A$ and $D = (x_D, y_D, z_i) \in l_B$, satisfying the equations:

  $$\|C - D\|^2 = \frac{(2\pi r_i)^2}{m^2}, \frac{\|A - D\|^2}{\|B - C\|^2} = \lambda^2.$$

  Update $A := C$ and $B := D$
end while
Obtain a strip bounded by l_A and l_B with similar inscribed parallelgromas (Fig. 11-(A));
Rotate the strip around the axis by a constant angle $\frac{2\pi}{m}$ to get the remaining $m - 1$ congruent strips;
Construct an I-net with $m \times n$ (θ, θ_0)−quads (Fig. 11-(B));
Extract two families of diagonals, which have constant angles with respect to the parallels and are thus also loxodromes.
Output: An isogonal 4-web with three families of loxodromes and a family of parallel circles covering the rotational surface, see Fig. 11-(C).

Table 1
Optimization statistics implemented in Python on a 2.7 GHz Intel® Core i5 CPU with 8 GB RAM. The initial meshes have unit diagonal length in their bounding boxes. For the last two iterations, the weights for fairness ω_2, self-closeness ω_3, and mesh approximation ω_4 are set to zero. For all previous iterations, the weights are set as $\omega_2 = 0.005$ and $\omega_3 = \omega_4 = 0.01$.

Figs.	$\|F\|$	*#var*	*#cons*	*residual*	*#iter*	Time [s]/it
Fig. 12						
(A)	400	3728	3201	1.2*e*−12	12	0.127
(B)	400	3728	3601	3.1*e*−12	17	0.121
(C)	400	3728	3601	2.9*e*−13	17	0.122
(D)	400	2126	1602	1.6*e*−12	17	0.107
(E)	400	2126	1602	1.1*e*−8	17	0.116
Fig. 13						
(A)	433	2323	1730	3.6*e*−12	12	0.17
(B)	433	4052	4321	3.8*e*−10	12	0.165

References

[1] Bommes D, Lévy B, Pietroni N, Puppo E, Silva C, Tarini M, Zorin D. Quad-mesh generation and processing: A survey. In: Computer Graphics Forum. 32, 2013, p. 51–76.
[2] Pottmann H, Eigensatz M, Vaxman A, Wallner J. Architectural geometry. Comput Graph 2015;47:145–64.
[3] Adriaenssens S, Block P, Veenendaal D, Williams C. Shell structures for architecture: form finding and optimization. Routledge; 2014.
[4] Dellinger F, Li X, Wang H. Discrete orthogonal structures. Comput Graph 2023;114:126–37.
[5] Pellis D, Pottmann H. Aligning principal stress and curvature directions. In: Advances in Architectural Geometry. Klein Publ. Ltd; 2018.
[6] Li Z, Lee T, Pietroni N, Snooks R, Xie YM. Design and construction of catenary-ruled surfaces. Structures 2024;59:105755.
[7] Jimenez MR, Müller C, Pottmann H. Discretizations of surfaces with constant ratio of principal curvatures. Discrete Comput Geom 2020;63:670–704.
[8] Jiang C, Wang C, Schling E, Pottmann H. Computational design and optimization of quad meshes based on diagonal meshes. In: Advances in Architectural Geometry. Presses des Ponts; 2021.

[9] Wang H, Pottmann H. Characteristic parameterizations of surfaces with a constant ratio of principal curvatures. Comput-Aided Geom Des 2022;93.
[10] Pellis D, Wang H, Rist F, Kilian M, Pottmann H, Müller C. Principal symmetric meshes. ACM Trans Graph 2020;39(4):127:1–7.
[11] Pellis D, Kilian M, Wang H, Jiang C, Müller C, Pottmann H. Architectural freeform surfaces designed for cost-effective paneling mold re-use. In: Advances in Architectural Geometry. 2020.
[12] Schling E, Wang H, Hoyer S, Pottmann H. Designing asymptotic geodesic hybrid gridshells. Comput- Aided Des 2022;152:103378.
[13] Schling E, Wan Z, Wang H, D'Acunto P. Asymptotic geodesic hybrid timber gridshell. In: Advances in Architectural Geometry. Berlin/Boston: De Gruyter; 2023.
[14] Jiang C, Wang C, Rist F, Wallner J, Pottmann H. Quad-mesh based isometric mappings and developable surfaces. ACM Trans Graph 2020;39(4):128:1–3.
[15] Jiang C, Wang H, Ceballos Inza V, Dellinger F, Rist F, Wallner J, Pottmann H. Using isometries for computational design and fabrication. ACM Trans Graph 2021;40(4):42:1–12.
[16] Schling E, Kilian M, Wang H, Schikore D, Pottmann H. Design and construction of curved support structures with repetitive parameters. In: Advances in Architectural Geometry. Klein Publ. Ltd; 2018.
[17] Kilian M, Wang H, Schling E, Schikore J, Pottmann H. Curved support structures and meshes with spherical vertex stars. In: ACM SIGGRAPH posters. Association for Computing Machinery; 2018.
[18] Jiang C, Peng C-H, Wonka P, Pottmann H. Checkerboard patterns with black rectangles. ACM Trans Graph 2019;38(6):171:1–3.
[19] Pottmann H, Asperl A, Kililan A. Architectural geometry. SIAM; 2007.
[20] Dellinger F. The discrete differential geometry of checkerboard patterns (Ph.D. thesis), TU Wien; 2024.
[21] Jiang C, Lyakhov D, Rist F, Pottmann H, Wallner J. Quad mesh mechanisms. ACM Trans Graph 2024;43(6):243:1–17.
[22] Tang C, Sun X, Gomes A, Wallner J, Pottmann H. Form-finding with polyhedral meshes made simple. ACM Trans Graph 2014;33(4):70:1–9.
[23] Bobenko AI, Suris YB. Discrete differential geometry. Integrable structure. Graduate studies in mathematics, 98, American Mathematical Society, Providence, RI; 2008.
[24] Crane K. Conformal geometry of simplicial surfaces. In: Proceedings of symposia in applied mathematics. American Mathematical Society; 2020.
[25] Gu X, Yau S-T. Computational conformal geometry. International Press of Boston, Inc; 2008, p. 295.
[26] Monge G. Applications de l'analyse à la géométrie. Bachelier; 1850, p. 609–17, Contains J. Liouville's 'Extension au cas des trois dimensions de la question du tracé géographique' as Note VI.
[27] Ahlfors L. Mobius transformations in several dimensions. Lect Notes Univ Minn 1981.
[28] Wikipedia. Varignon's theorem. 1731, URL https://en.wikipedia.org/wiki/Varignon%27s_theorem.
[29] Wang H, Pellis D, Rist F, Pottmann H, Müller C. Discrete geodesic parallel coordinates. ACM Trans Graph 2019;(6):38:1–13.
[30] Bo P, Wang W. Geodesic-controlled developable surfaces for modeling paper bending. In: Computer Graphics Forum. 26, 2007, p. 365–74.
[31] do Carmo M. Differential geometry of curves and surfaces. Prentice-Hall; 1976.
[32] Pottmann H, Wallner J. Computational line geometry. Berlin, Heidelberg: Springer-Verlag; 2001.
[33] Aksoyak FK, Demirci BB, Babaarslan M. Characterizations of loxodromes on rotational surfaces in Euclidean 3-space. Int Electron J Geom 2023;16(1):147–59.
[34] Wang B, Wang H, Schling E, Pottmann H. Rectifying strip patterns. ACM Trans Graph 2023;42(6):256:1–18.
[35] Pottmann H, Jiang C, Höbinger M, Wang J, Bompas P, Wallner J. Cell packing structures. Comput- Aided Des 2015;60:70–83.
[36] Vaxman A, Müller C, Weber O. Regular meshes from polygonal patterns. ACM Trans Graph 2017;36(4):113:1–5.
[37] Xu Q-C, Deng B, Yang Y-L. Ellipsoid packing structures on freeform surfaces. In: Computer Graphics Gorum. 37, 2018, p. 87–95.
[38] Jiang C, Rist F, Wang H, Wallner J, Pottmann H. Shape-morphing mechanical metamaterials. Comput- Aided Des 2022;143.
[39] Tian L, Sun B, Yan X, Sharf A, Tu C, Lu L. Continuous transitions of triply periodic minimal surfaces. Addit Manuf 2024;84:104105.
[40] Oehri A, Segall A, Ren J, Sorkine-Hornung O. Chebyshev parameterization for woven fabric modeling. ACM Trans Graph 2024;43(6):205:1–15.